The 1998 eruption of Axial Seamount: New insights on submarine lava flow emplacement from high-resolution mapping

Citation	Chadwick, W. W., et al. (2013), The 1998 eruption of Axial Seamount: New insights on submarine lava flow emplacement from high-resolution mapping, Geochemistry Geophysics Geosystems, 14, 3939–3968. doi:10.1002/ggge.20202
DOI	10.1002/ggge.20202
Publisher	American Geophysical Union
Version	Version of Record
Citable Link	http://hdl.handle.net/1957/47237
Terms of Use	http://cdss.library.oregonstate.edu/sa-termsofuse

Geochemistry Geophysics Geosystems G3

Article
Volume 14, Number 10
2 October 2013
doi: 10.1002/ggge.20202
ISSN: 1525-2027

Published by AGU and the Geochemical Society

The 1998 eruption of Axial Seamount: New insights on submarine lava flow emplacement from high-resolution mapping

W. W. Chadwick Jr.
Hatfield Marine Science Center, CIMRS, Oregon State University, 2115 SE OSU Drive, Newport, Oregon, 97365, USA (bill.chadwick@oregonstate.edu)

D. A. Clague
Monterey Bay Aquarium Research Institute, Moss Landing, California, USA

R. W. Embley
NOAA/PMEL, Newport, Oregon, USA

M. R. Perfit
Department of Geological Sciences, University of Florida, Gainesville, Florida, USA

D. A. Butterfield
JISAO, University of Washington, Seattle, Washington, USA

D. W. Caress, J. B. Paduan, and J. F. Martin
Monterey Bay Aquarium Research Institute, Moss Landing, California, USA

P. Sasnett
Department of Geological Sciences, University of Canterbury, Christchurch, New Zealand

S. G. Merle and A. M. Bobbitt
Hatfield Marine Science Center, CIMRS, Oregon State University, Newport, Oregon, USA

[1] Axial Seamount, an active submarine volcano on the Juan de Fuca Ridge at 46°N, 130°W, erupted in January 1998 along 11 km of its upper south rift zone. We use ship-based multibeam sonar, high-resolution (1 m) bathymetry, sidescan sonar imagery, and submersible dive observations to map four separate 1998 lava flows that were fed from 11 eruptive fissures. These new mapping results give an eruption volume of 31×10^6 m^3, 70% of which was in the northern-most flow, 23% in the southern-most flow, and 7% in two smaller flows in between. We introduce the concept of map-scale submarine lava flow morphology (observed at a scale of hundreds of meters, as revealed by the high-resolution bathymetry), and an interpretive model in which two map-scale morphologies are produced by high effusion-rate eruptions: "inflated lobate flows" are formed near eruptive vents, and where they drain downslope more than 0.5–1.0 km, they transition to "inflated pillow flows." These two morphologies are observed on the 1998 lava flows at Axial. A third map-scale flow morphology that was not produced during this eruption, "pillow mounds," is formed by low effusion-rate eruptions in which pillow lava piles up directly over the eruptive vents. Axial Seamount erupted again in April 2011 and there are remarkable similarities between the 1998 and 2011 eruptions, particularly the locations of eruptive vents and lava flow morphologies. Because the 2011 eruption reused most of the same eruptive fissures, 58% of the area of the 1998 lava flows is now covered by 2011 lava.

Components: 19,282 words, 16 figures, 2 tables.

Keywords: submarine eruption; high-resolution bathymetry; lava flow morphology.

Index Terms: 8429 Lava rheology and morphology: Volcanology; 8416 Mid-oceanic ridge processes: Volcanology; 8427 Subaqueous volcanism: Volcanology; 8414 Eruption mechanisms and flow emplacement: Volcanology.

Received 27 February 2013; **Revised** 14 May 2013; **Accepted** 11 June 2013; **Published** 2 October 2013.

Chadwick, W. W., et al. (2013), The 1998 eruption of Axial Seamount: New insights on submarine lava flow emplacement from high-resolution mapping, *Geochem. Geophys. Geosyst.*, *14*, 3939–3968, doi:10.1002/ggge.20202.

1. Introduction

[2] Axial Seamount (Figure 1a) is an active submarine volcano located on the Juan de Fuca Ridge (JdFR), a spreading center in the northeast Pacific Ocean [*Johnson and Embley*, 1990]. It is the current location of the Cobb hotspot, which provides an enhanced magma supply, and gives it characteristics of both a mid-ocean ridge segment and a hotspot volcano [*Desonie and Duncan*, 1990; *Rhodes et al*., 1990; *Chadwick et al*., 2005]. The youngest volcanism at Axial has occurred in its summit caldera (8 km × 3 km) and along its two rift zones that extend to the north and south [*Appelgate*, 1990; *Embley et al*., 1990; *Clague et al*., 2013]. Of the two rift zones, the south rift has been the most active since the caldera formed, because south rift lavas bury the SE sector of the caldera fault, which is up to 100 m high elsewhere (Figure 1b). Long-lived, high-temperature hydrothermal vents (both metal-rich sulfide and metal-poor anhydrite chimneys) are localized near the caldera-bounding ring faults (Figure 1b). Lower temperature diffuse vent sites are found in proximity to the high-T vents and also along the rift zones where they are more prone to perturbation by eruptions [*Embley et al*., 1990; *Butterfield et al*., 2004].

[3] Axial Seamount erupted in January 1998 [*Embley et al*., 1999] and most recently in April 2011 [*Caress et al*., 2012; *Chadwick et al*., 2012; *Dziak et al*., 2012], and both eruptions were along the south rift zone. As such, Axial is one of only three locations on the global mid-ocean ridge where historical submarine eruptions are known to have recurred (the others being the CoAxial segment of the JdFR [*Chadwick et al*., 1995; *Embley et al*., 2000] and the East Pacific Rise at 9–10°N [*Haymon et al*., 1993; *Rubin et al*., 1994; *Soule et al*., 2009; *Fundis et al*., 2010]). This paper will focus on the lava flows produced in 1998 at Axial, which have not previously been described in detail. The earthquakes associated with the 1998 eruption were detected acoustically by the hydrophone arrays of the U.S. Navy's SOund SUrveillance System (SOSUS) [*Dziak and Fox*, 1999]. What is unique about the 1998 Axial eruption is that seafloor-monitoring instruments were in place during the event that shed light on the sequence of events [*Baker et al*., 1999; *Chadwick et al*., 1999b; *Embley and Baker*, 1999; *Fox*, 1999; *Fox et al*., 2001; *Chadwick*, 2003]. These data sets, combined with previously unpublished high-resolution bathymetry and near-bottom observations from submersible and remotely operated vehicle (ROV) dives, give new insights into the distribution, morphology, and emplacement processes of the 1998 lava flows, and how they varied with location, slope, and distance from the vents.

2. Methods

2.1. Ship-Based Multibeam Sonar Surveys

[4] One of the first methods employed for mapping the 1998 lava flows was a ship-based multibeam sonar resurvey of the summit and south rift zone where the earthquake swarm had migrated southward a distance of 50 km [*Dziak and Fox*, 1999]. Pre-eruption non-GPS navigated bathymetry collected in 1981, 1991, and 1996 (12 kHz Seabeam and Hydrosweep sonars) was compared to a GPS-navigated post-eruption survey in May 1998 (30 kHz EM300 sonar) [*Embley et al*., 1999]. This comparison found an area of barely detectable depth change (≤13 m) at the southern end of the northern-most 1998 flow (near 45° 54.7′N) and a larger, more distinct anomaly of ≤26 m over the southern-most 1998 flow (near 45° 52.1′N). These depth changes were later confirmed to be the two

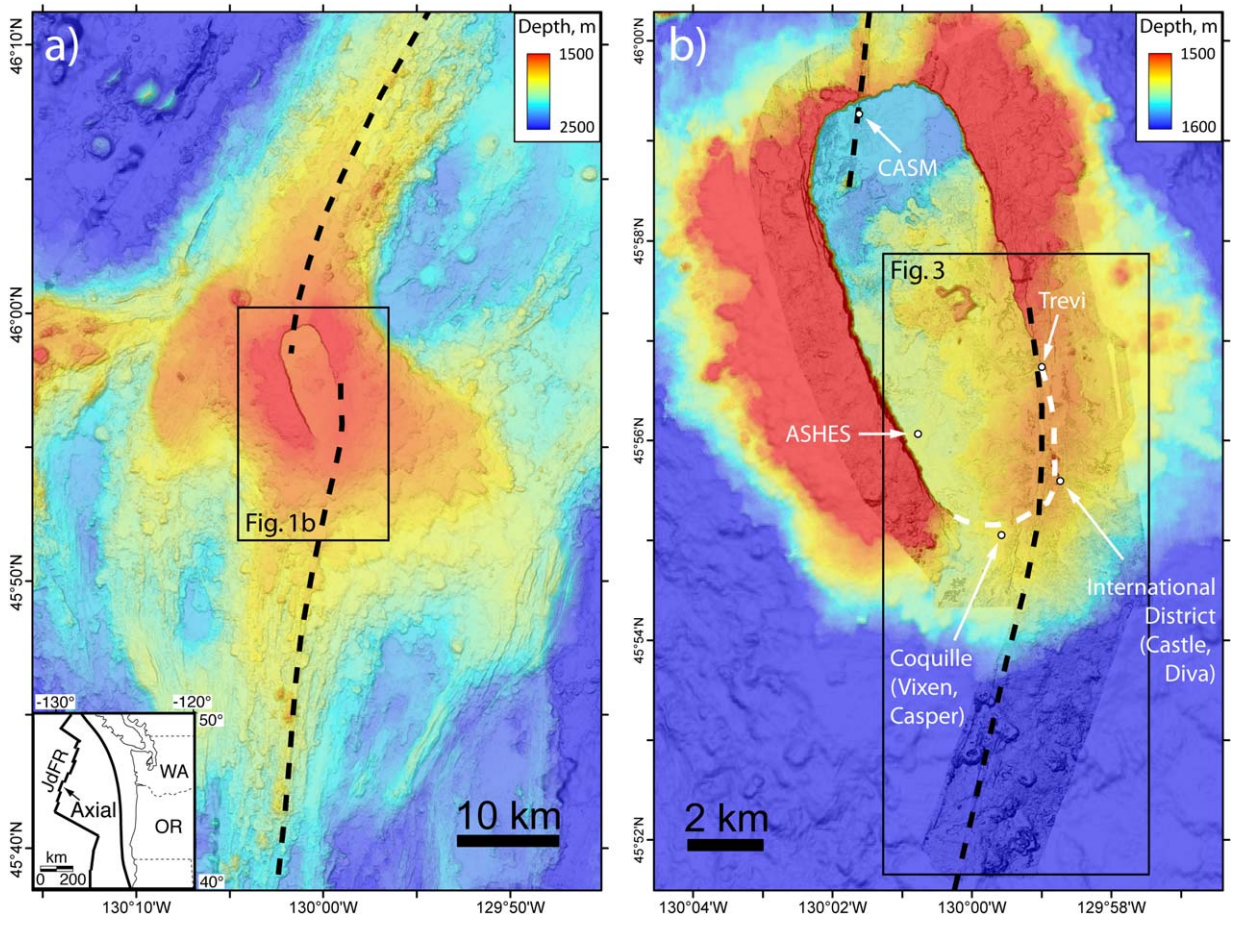

Figure 1. Location maps of Axial Seamount in the NE Pacific (inset). (a) The summit caldera and north and south rift zones (black dashed lines) are prominent in regional bathymetry (25 m grid). (b) A more detailed map of the summit shows that recent eruptions from the upper south rift zone have buried the caldera fault (white dashed line) in the SE part of the caldera. High-temperature hydrothermal vent sites (white labeled dots) are located near the caldera fault or its buried extension. MBARI AUV bathymetry (1 m grid) over ship-based bathymetry (25 m grid). Black boxes show locations of other figures.

main areas of eruption in 1998 by observations made during submersible dives. Despite the earthquake evidence that a dike intruded as far south as 45° 27′N [*Dziak and Fox*, 1999; *Embley et al.*, 1999], there was no indication that any lava erupted south of 45° 51′N from the repeat mapping or from water column surveys during an event-response cruise in February 1998 [*Baker et al.*, 1999; *Lupton et al.*, 1999; *Resing et al.*, 1999]. There is admittedly some ambiguity here, since the pre-eruption bathymetry was navigated less precisely and lower in resolution, and the event-response CTD casts were sparse, but nevertheless any eruption on the south rift zone in 1998 of significant size (> 15 m thick) should have been detected by these methods. In sum, the available evidence suggests that 1998 dike apparently only erupted along 1/5 of its seismically determined length.

2.2. Sidescan Sonar Imagery

[5] The summit and rift zones of Axial Seamount were surveyed with 30 kHz Sea MARC I deep-towed sidescan sonar in 1982 and 1985–1987 [*Appelgate*, 1990; *Embley et al.*, 1990] and these data provide key pre-eruption imagery of the seafloor that help to identify the extent of 1998 lava flows in some areas. The 1982 sidescan survey produced analog data output (hard copy only), whereas the 1985–1987 surveys were digital. In this paper, we only show the digital data, but all the features we refer to in the 1985–1987 imagery are also visible in the 1982 survey. Sidescan data were collected with different swath-widths (500 m, 1 km, 2 km, and 5 km) and resolutions (0.5 m, 1 m, 2 m, and 5 m, respectively). The original pre-GPS navigation of the sidescan data is relatively poor and is compounded by uncertainty in the towfish location [*Appelgate*, 1990;

Embley et al., 1990]. The sidescan data presented here have been shifted rigidly to match distinctive features in more recent GPS-navigated bathymetry. Nevertheless, there are still navigation errors of up to ~50 m.

2.3. Alvin and ROV Dives

[6] Our primary tools for making visual observations of the seafloor were submersible and ROV dives, which allowed us to delineate contacts between 1998 flows and the older surrounding lavas, map the distribution of lava morphologies and collapse areas, and track the evolution of hydrothermal venting over time associated with the new lavas. The first dives after the January 1998 eruption were made in July 1998 with the submersible *Alvin* and in August 1998 with the ROV *ROPOS* [*Embley and Baker*, 1999; *Embley et al*., 1999]. Subsequent ROV dives for geologic mapping were made with *ROPOS* in the summers of 1999–2004 and 2006, with *Tiburon* in 2005, *Doc Ricketts* in 2009 and 2011, and with *Jason* in 2007, 2010, and 2011. These dives had multiple purposes including studying biological succession [*Marcus and Hourdez*, 2002; *Marcus et al*., 2009], vent fluid sampling [*Butterfield et al*., 2004], and geophysical monitoring [*Chadwick et al*., 2006; *Nooner and Chadwick*, 2009], but having them spread over a decade allowed us to expand the geologic mapping incrementally and track age-related changes over time. Such multiyear observations were made possible because Axial was the location of NOAA's NeMO seafloor observatory (http://www.pmel.noaa.gov/vents/nemo/) and has been chosen to be a node on NSF's regional cabled observatory in the NE Pacific as part of the Ocean Observatories Initiative (http://www.interactiveoceans.washington.edu/). Acoustic navigation for the earlier ROV dives was accomplished with networks of expendable long-baseline (LBL) transponders, one in place from 1998 to 2003 and another between 2003 and 2007, and since 2007 by ultrashort baseline navigation (USBL). The long-lived transponder networks kept navigation consistent from year to year, but modern USBL systems have better repeatability (±40 m versus ± 10 m).

2.4. High-Resolution Bathymetry

[7] The most important mapping tools were sonars that collected high-resolution (1–2 m) bathymetry, allowing the structure, topography, and morphology of the seafloor to be visualized in fine detail. Such high-resolution bathymetry is extremely valuable for geologic mapping purposes, because it fills an observational gap between ROV video and ship-based bathymetry, and allows near-bottom geologic observations to be placed in a meaningful spatial context. High-resolution mapping was started at Axial using an Imagenex (675 kHz) scanning sonar mounted on the ROVs *ROPOS* and *Jason*, which collected bathymetry over part of the 1998 eruption site during 21 dives between 1998 and 2001, following the methods described in *Chadwick et al*. [2001]. The scanning sonar data were gridded at 2–5 m resolution and although the density of the sonar soundings is variable they provided an adequate basemap for early stages of geologic mapping [*Embley et al*., 1999; *Fox et al*., 2001; *Chadwick et al*., 2002; *Chadwick*, 2003].

[8] Between 2006 and 2009, the entire summit of Axial Seamount was mapped at 1 m resolution by the Autonomous Underwater Vehicle (AUV) *D. Allan B*., operated by the Monterey Bay Aquarium Research Institute (MBARI) [*MBARI*, 2001; *Caress et al*., 2007; *Clague et al*., 2007; *Clague et al*., 2013]. These 200 kHz multibeam sonar data were used as a pre-eruption surface and compared with a post-eruption survey to reveal depth changes due to the April 2011 lava flows [*Caress et al*., 2012]. The MBARI AUV was navigated by a combination of USBL positioning, inertial navigation, Doppler velocity log, and feature matching during data postprocessing, as described in *Caress et al*. [2008]. The AUV bathymetry was also coregistered with ship-based EM300/EM302 multibeam bathymetry which are lower resolution but GPS-navigated, improving the AUV navigation accuracy in an absolute sense. The final AUV navigation is accurate in a relative sense to 1 m, in an absolute sense to 35 m (the lateral resolution of the ship-based bathymetry) and has a vertical precision of 0.1 m [*Caress et al*., 2012]. Supporting information Figure S1[1] in the auxiliary material compares maps of ship-based EM300 multibeam data gridded at 25 m, Imagenex data gridded at 2 m, and MBARI AUV data gridded at 1 m. The Imagenex data were clearly a huge improvement from ship-based bathymetry, but the MBARI AUV data are far superior for geologic mapping because of their higher data density, resolution, and improved navigation.

2.5. Relation to Previous Studies

[9] Many previous studies have used ship-based multibeam sonar, sidescan sonar, camera tows,

[1]Additional supporting information may be found in the online version of this article.

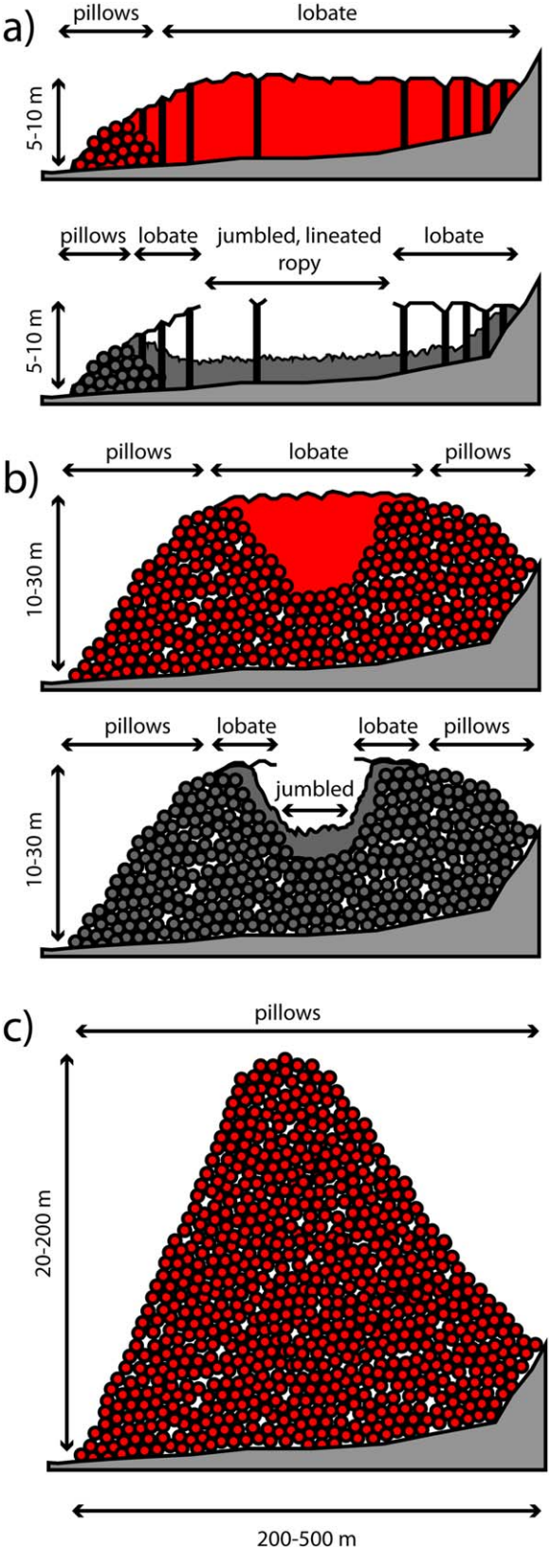

and/or submersible dive observations to conduct geologic mapping of young lava flows on the seafloor [*Ballard and van Andel*, 1977; *Ballard et al*., 1979; *Crane and Ballard*, 1981; *Ballard et al*., 1984; *Smith and Cann*, 1992; *Haymon et al*., 1993; *Chadwick and Embley*, 1994; *Embley and Chadwick*, 1994; *Chadwick et al*., 1998; *Embley et al*., 2000; *White et al*., 2000; *Sinton et al*., 2002; *Cormier et al*., 2003; *Fornari et al*., 2004; *Soule et al*., 2005, 2007; *White et al*., 2008; *Soule et al*., 2009; *Fundis et al*., 2010]. However, Axial Seamount was the first place where the entire area of historically erupted lavas was mapped with 1 m resolution, AUV-based multibeam bathymetry. This high-resolution view of the seafloor, combined with in-situ monitoring instrument observations, provides new insights about how the lavas were emplaced and the role of emplacement history on lava flow morphology. The petrology and geochemistry of the 1998 lava flows are described in *Chadwick et al*. [2005] and *Clague et al*. [2013].

3. Results

3.1. Submarine Lava Flow Terminology

[10] Before presenting our mapping results, a review of the terminology we will use to describe submarine lava flow morphology is needed. In this paper, we distinguish between "photo-scale" lava morphology (at a scale of a few meters, based on observations from submersibles and imagery from camera-tows or ROV video) and "map-scale" flow morphology (at a scale of hundreds of meters and discernable in the AUV bathymetry). At the photo-scale, we follow previously used descriptive terminology for lava morphology in a spectrum

Figure 2. Cartoon cross sections showing map-scale flow morphologies discussed in the text: (a) Inflated lobate flow, (b) inflated pillow flow, and (c) pillow mound. Note horizontal scale at bottom is 200–500 m for all flow types but their thicknesses differ. Red shows areas of molten lava when flows are fully inflated; dark grey shows solidified lava after drain out; black shows solid crusts on individual pillows (small circles), inflated flow interiors (in Figures 2a and 2b), and on lava pillars (vertical lines in Figure 2a). Labeled arrows show differing distributions of photo-scale lava morphologies (pillows, lobate, jumbled, etc). Supporting information Animation S1 shows the emplacement of an inflated lobate flow. The Axial 1998 lava flows exhibit "inflated lobate flow" morphology near the eruptive vents and "inflated pillow flow" morphology at the distal ends of flows, separated by a channelized transitional zone on slopes (see Figure 3a).

from pillows, to lobate lava, to sheets (including lineated, ropy, and jumbled or hackly, in order of increasing surface crust disruption) [*Fox et al*., 1988; *Perfit and Chadwick*, 1998; *Fundis et al*., 2010]. At the map-scale, we use the terms, "inflated lobate flows," "inflated pillow flows," and "pillow mounds" to describe flow morphologies with distinct characteristics, as shown in Figure 2. The key differences between them are flow thickness, existence and extent of molten lava cores during emplacement as reflected by collapsed areas, and the spatial distribution and proportion of photo-scale lava morphologies. We propose a conceptual model in which "pillow mounds" are created by low effusion-rate eruptions, the other two inflated flow types are produced by high effusion-rate eruptions, and "inflated lobate flows" and "inflated pillow flows" are near-vent and distal morphologies, respectively. We use the term "inflated" to refer to sheet-like flows that had a molten interior beneath a solidified crust during emplacement, analogous to the inflated pahoehoe flows on land described by *Hon et al*. [1994]. Inflated flows are initially thin and subsequently increase in thickness after they stop advancing laterally but while molten lava is still being added to the fluid interior of the flow from the eruptive vents [*Hon et al*., 1994; *Gregg and Chadwick*, 1996]. After this inflation phase, the still-molten interior of such flows may drain out downslope. Where drain out occurs on submarine inflated flows, it leads to collapse of the (now unsupported) upper solidified crust [*Engels et al*., 2003], and the degree of collapse reflects the previous areal extent of the molten flow core and the rate and amount of lava drain out (Figure 2).

[11] At the photo-scale, pillow lavas extrude as individual spherical or cylindrical tubes of lava that cool and crust over on all sides, generally preventing coalescence with neighboring pillows [*Moore*, 1975]. At the map-scale, "pillow mounds" are produced by the piling up of individual pillows [e.g., *Chadwick and Embley*, 1994; *White et al*., 2002; *Yeo et al*., 2012]; thus such mounds do not have a molten core, are usually thick and steep-sided, and form directly over their eruptive vents (Figure 2c). In contrast, "inflated lobate flows" initially advance one lobe at a time, but rapidly enough that the lobes quickly coalesce into one hydraulically connected flow beneath an upper crust that preserves the original lobate surface morphology. These flows commonly pond and inflate, producing relatively flat upper crusts that may later collapse if the molten interior of the flow drains out (Figure 2a). Such flows generally have lava pillars in their collapsed interiors [*Francheteau et al*., 1979], which are typically floored with a variety of sheet lava morphologies (at the photo-scale) that form during drain-out. At Axial, "inflated lobate flows" transition downslope to "inflated pillow flows" at the distal ends of flows, sometimes with an area of channelized sheet flows in between (Figure 3a). Compared to "inflated lobate flows," "inflated pillow flows" are thicker, have larger proportions of pillowed flow fronts and levees, and smaller collapse areas, reflecting smaller molten cores during emplacement (Figure 2b). Below, we describe the 1998 lava flows in more detail in the context of this conceptual model.

3.2. The Extent, Area, and Volume of 1998 Lavas

[12] Some of the primary results of this study are the location of the 1998 eruptive fissures and the mapped area and extent of the 1998 lavas (Figure 3a), which can be used to calculate the volume of the eruption. There were four separate lava flows erupted along Axial's upper south rift zone in 1998, a larger "Northern" flow that contains 70% of the erupted volume, and three smaller "Southern" flows, which contain, 6%, 1%, and 23% of the volume, respectively from north to south. The Northern flow was 7 km long and extended from 45° 53.8′–57.6′N, both inside and outside the caldera. The three Southern flows were erupted over a distance of 3.7 km and extended from 45° 51.8′–53.8′N, up to ~10 km from the center of the caldera along the south rift zone (Figure 3a).

[13] Several preliminary versions of the 1998 lava flow outlines have been previously published, based on the visual observations and Imagenex bathymetry that were available at the time [*Baker et al*., 1999; *Embley et al*., 1999; *Lupton et al*., 1999; *Fox et al*., 2001; *Tolstoy et al*., 2002; *Chadwick*, 2003; *Baker et al*., 2004; *Butterfield et al*., 2004; *Sohn et al*., 2004; *Chadwick et al*., 2006; *Huber et al*., 2006; *Gilbert et al*., 2007; *Marcus et al*., 2009; *Nooner and Chadwick*, 2009; *Opatkiewicz et al*., 2009]. However, the flow outlines we present here are significantly different and improved, because they are based on a new and better data synthesis, and they should supersede all previous versions. The earlier mapping was most complete in the central parts of the Northern lava

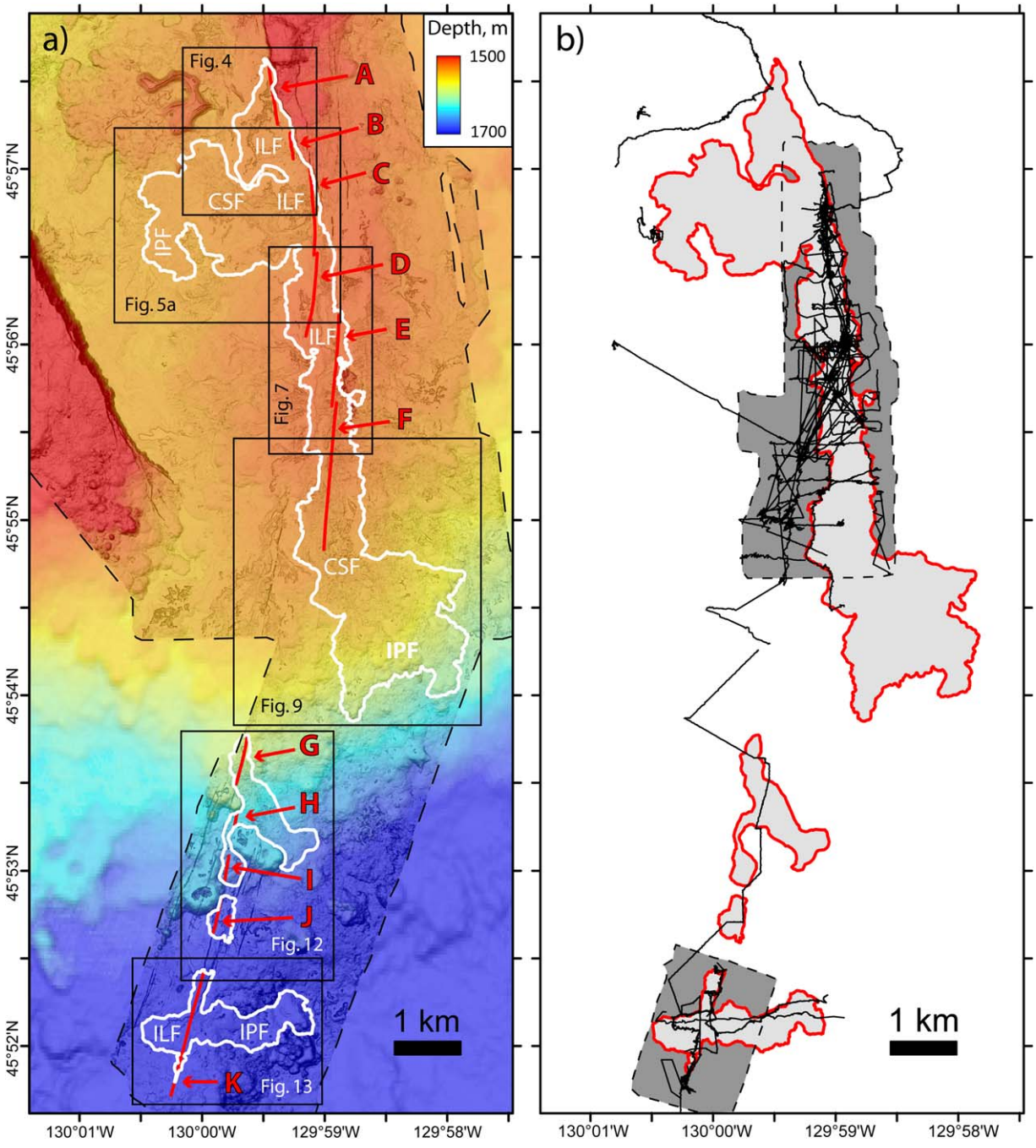

Figure 3. (a) Map showing the 1998 lava flows (white outlines) and eruptive fissures (red lines). Areas with distinctive map-scale flow morphologies are labeled as follows: ILF = inflated lobate flow; IPF = inflated pillow flow; CSF = channelized sheet flow (a transitional morphology between ILF and IPF). Extent of MBARI AUV bathymetry (1 m grid) is shown by dashed black line, and overlies ship-based EM300 bathymetry (25 m grid). Black boxes show locations of other figures. (b) Map showing submersible dive tracks (black lines) and areas of Imagenex scanning sonar bathymetry (dark grey with dashed outlines) that were used to help map the 1998 lava flow contacts (light grey with red outlines). Tracks include *Alvin* dives 3245 and 3247, *ROPOS* dives 460, 461, 464, 465, 473, 474, 478, 488, 491, 492, 493, 494, 495, 496, 501, 546, 552, 554, 627, 630, 1010, 1011, 1012, *Tiburon* dive 874, *Doc Ricketts* dives 73, 74, 79, 270, and *Jason* dives 289, 291, 292.

flow and the largest Southern flow, where submersible dive tracks were densest and where Imagenex bathymetry existed (Figure 3b). The early flow outlines were most uncertain where dives and Imagenex data were sparse or nonexistent at the north and south ends of the Northern

Table 1. Thicknesses, Areas, and Volumes of 1998 Lava Flows at Axial Seamount

Eruption Site	Maximum Depth Change From Ship-Based Multibeam Comparison (m)	Area of Ship-Based Multibeam Depth Changes Only ($\times 10^6$ m^2)[a]	Volume of Ship-Based Multibeam Depth Changes Only ($\times 10^6$ m^3)[a]	Total Mapped Area of 1998 Lava ($\times 10^6$ m^2)[b]	Estimated Total Volume of 1998 Lava Erupted ($\times 10^6$ m^3)[c]
Northern 1998 flow "A–F"	13	0.52	3.4	5.8	21.8
Southern 1998 flow "G–I"	n/a	n/a	n/a	0.54	1.9
Southern 1998 flow "J"	n/a	n/a	n/a	0.09	0.3
Southern 1998 flow "K"	26	0.49	6.2	0.72	7.0
Total	26	1.1	9.6	7.1	31.0

[a]The areas and volumes of multibeam depth changes were calculated from the depth difference grids. These numbers are minimums because substantial parts of the 1998 lava flows were below the detection threshold of this technique.
[b]The total flow areas are calculated from the mapped extent of the lava flows using ArcGIS software.
[c]The total volume of lava erupted is calculated by multiplying the "missing" area (the difference between the total flow area and the area of the ship-based multibeam depth changes) by a constant thickness of 3.5 m (the average thickness for the 2011 lava flows erupted in and near the caldera from *Caress et al*. [2012]), and adding this "missing" volume to the volume of ship-based multibeam depth changes.

flow. Most importantly, the new flow outlines benefit from the higher-resolution MBARI AUV bathymetry and comparison with the pre-eruption sidescan sonar imagery.

[14] The high-resolution of the MBARI AUV bathymetry also allowed mapping of 11 separate eruptive fissures that fed the 1998 lava flows, which we distinguish by letter designations A–K, from north to south (Figure 3a). The eruptive fissures were identified in the AUV bathymetry by narrow linear collapses that coincide with local highs in relatively uncollapsed areas, or by troughs in areas where more extensive lava drain-out and collapse had occurred. The eruptive fissures extended over a distance of 11 km, with a gap of 2.1 km between the northern (A–F) and southern (G–K) fissures. Their orientation rotated from 353° at the north end (parallel to the nearby caldera wall) to 015° at the south end (the trend of the south rift zone outside the caldera).

[15] The new outline of the Northern lava flow has an area of 5.8 $\times$ 10^6 m^2 and the areas of the three Southern flows are 5.4 $\times$ 10^5 m^2, 0.9 $\times$ 10^5 m^2, and 7.2 $\times$ 10^5 m^2, for a total combined area of 7.1 $\times$ 10^6 m^2 (Table 1). To calculate the volume of the 1998 lava flows, we used the following method: (1) we started with the volumes of the depth differences from the pre-eruption and post-eruption ship-based multibeam comparison, and (2) to that we added the product of an average thickness times the area of the flow outlines, minus the area of the multibeam anomalies (which are already accounted for in step 1). In step 2, above, we used an average lava flow thickness of 3.5 m for the lavas not detected by multibeam differencing (the average thicknesses calculated by *Caress et al*. [2012] for the lava flows produced by the 2011 eruption in the same area). Following this method, we calculate a volume of 22 $\times$ 10^6 m^3 for the Northern flow, and 1.9 $\times$ 10^6 m^3, 3.1 $\times$ 10^5 m^3, and 7.0 $\times$ 10^6 m^3 for the three Southern flows, for a total 1998 lava flow volume of 31 $\times$ 10^6 m^3 (Table 1). This is within the range of 18–50 $\times$ 10^6 m^3 previously estimated by *Embley et al*. [1999], yet it is only 31% of the volume of lava erupted in 2011 [*Caress et al*., 2012].

3.3. The Northern 1998 Lava Flow

[16] The Northern 1998 lava flow can be geographically divided into northern, middle, and southern parts that have similar morphologies and emplacement histories. The Northern 1998 lava flow was fed from 6 *en echelon* eruptive fissures, A–F from north to south.

3.3.1. North Part of the Northern 1998 Lava Flow

[17] The north end of the Northern 1998 lava flow (north of ~45° 56.4′N) was erupted from three fissures that were located on the caldera floor close to the caldera-bounding fault, and none extended up onto the caldera rim (Figure 4a). The northernmost two eruptive fissures (A–B; 1 km in combined length) fed inflated lobate flows that extended up to 600 m to the west, with sinuous collapses in the cores of the flows that were apparently the axes of the lava distributary system, analogous to skylights above lava tubes on land [*Fornari*, 1986; *Peterson et al*., 1994]. The existence of 1998 lava flows in this area was unknown until the MBARI AUV bathymetry (Figure 4a) was compared to SeaMARC I sidescan sonar data (Figure 4b), which revealed that distinctive collapse features in the pre-eruption sidescan imagery were buried by 1998 lava in the post-eruption bathymetry. In this paper, sidescan imagery is

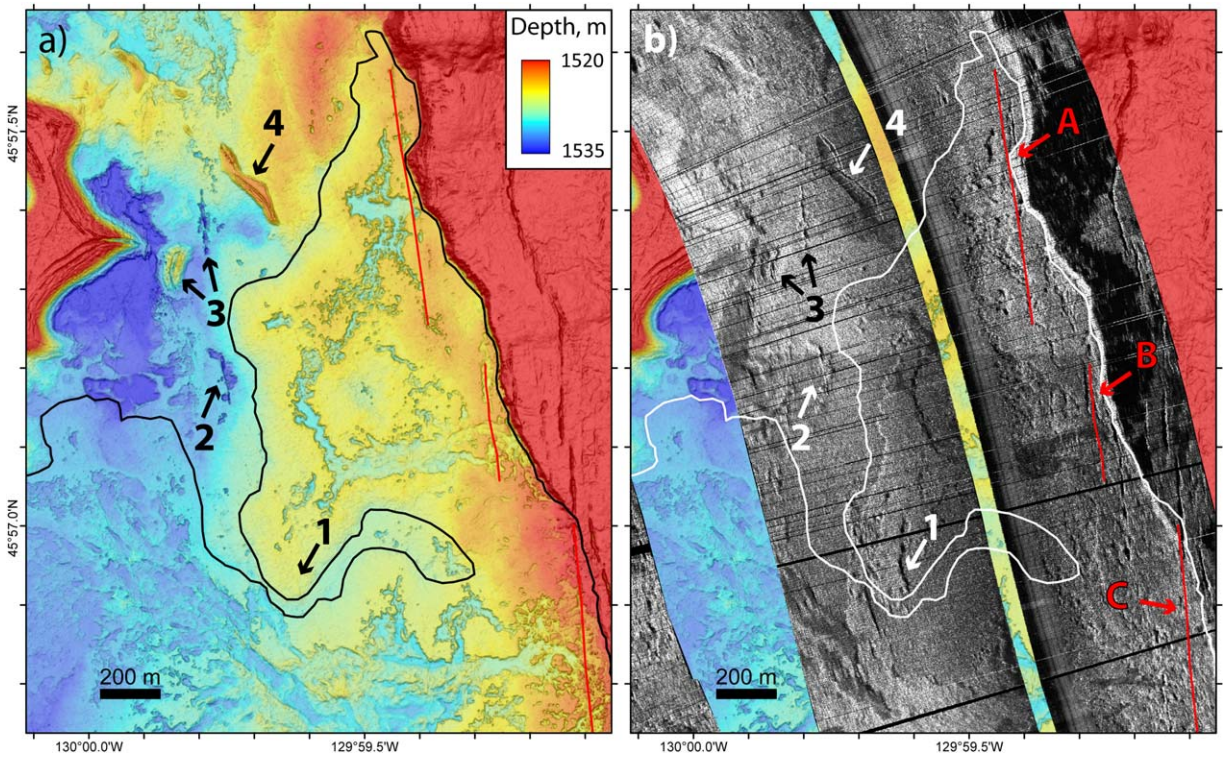

Figure 4. Map of the north end of the Northern 1998 lava flow, outlined (a) in black and (b) in white. (a) AUV bathymetry alone, and (b) overlain with pre-eruption sidescan sonar imagery (1 km swath) collected in 1985 (white is high backscatter; black is low backscatter). Channelized collapse feature (in Figure 4b), labeled 1, is clearly buried by 1998 lava in the post-eruption AUV bathymetry (in Figure 4a). In contrast, features labeled 2–4 are present in both maps and therefore were unburied by 1998 lava. Interpreted 1998 eruptive fissures (A–C) are shown as red lines, and labeled in Figure 4b.

displayed such that features with high-reflectivity (such as fault scarps) are white and those with low-reflectivity (such as acoustic shadows) are black.

[18] A small embayment of older unburied seafloor separates the lava flows that erupted from fissures B and C (Figures 4 and 5). Eruptive fissure C was originally mapped as the northern limit of the 1998 eruption [*Embley et al*., 1999], but the distance that lava flowed from this fissure to the west was unknown until we compared the post-eruption AUV bathymetry (Figure 5a) and the pre-eruption sidescan imagery (Figure 5b), which revealed that 1998 lava extends 1.8 km into the central caldera. In the pre-eruption sidescan imagery (Figure 5b), dark low-reflectivity areas in the central caldera are interpreted to be patches of flat lineated sheet flow in the floors of lava channels (their flat surfaces do not reflect much acoustic energy back to the sidescan towfish, in comparison to rougher jumbled or pillowed lava) [*Embley et al*., 1990; *Chadwick et al*., 1999a; *Soule et al*., 2005]. One large (100 × 500 m) and distinctively-shaped area of low-reflectivity in the sidescan imagery (labeled "1" in Figure 5b, and "lava pond" in Figure 9b of *Embley et al*. [1990]) is clearly buried by a large inflated lobe of lava in the post-1998 AUV bathymetry (Figure 5a). In Figures 4 and 5, we have also labeled other distinctive features that are visible in both the AUV bathymetry and the sidescan imagery, and are therefore unburied by 1998 lava, to help visually compare the maps.

[19] The large western lava lobe in Figure 5a was fed by a braided channel system from eruptive fissure C near the caldera wall. The difference in depth between the eruptive fissures and the distal edge of the large western lobe is 15–20 m, a slope of 0.5° (supporting information Figure S2a). Within 1 km of the eruptive fissure, the lavas are lobate and sheet flows with a prominent central channel and extensive areas of drain-out and collapse, 4–5 m deep (Figures 6a and 6b). Beyond that distance the lavas transition into a single inflated lobe of lava more than 5 m thick and without collapse features (supporting information

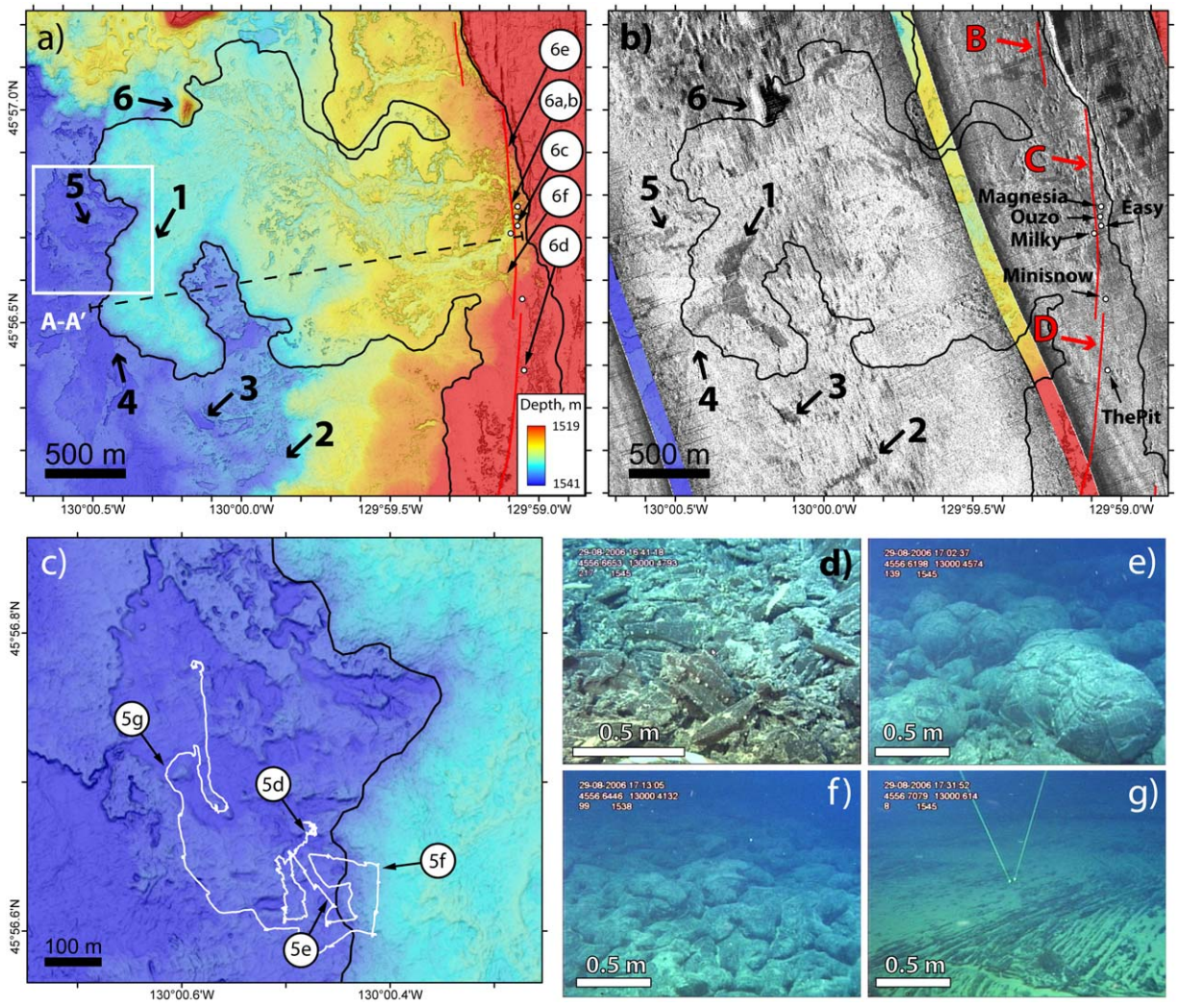

Figure 5. Map of the northwest part of the Northern 1998 lava flow (black outline). (a) AUV bathymetry alone and (b) overlain with pre-eruption sidescan sonar imagery (2 km swath) collected in 1985. Note dark, low-backscatter area labeled 1 in Figure 5b, interpreted to be flat lineated sheet lava, that is clearly buried by 1998 lava in Figure 5a. In contrast, features labeled 2–6 are present in both maps and therefore were unburied by 1998 lava. Interpreted 1998 eruptive fissures (B–D) are shown as red lines, (labeled in Figure 5b). White dots are snowblower vents Magnesia, Ouzo, Easy, Milky, Minisnow, and The Pit (labeled in Figure 5b). Dashed line A–A′ in Figure 5a is depth profile in supporting information Figure S2a. Circled numbers show locations of images in Figure 6. (c) Detail of the western edge of the 1998 flow (location shown by white box in Figure 5a) with the track of *ROPOS* dive R1010 (white line), which crossed the flow boundary in 2006. Circled numbers show locations of images in Figures 5d–5f. (d) Older jumbled lava with sponges (white dots) west of 1998 lava. (e) Contact of 1998 pillows over jumbled lava (foreground). (f) Lobate 1998 lava near top of inflated pillow flow. (g) Older flat lineated sheet lava in the floor of a collapse area. White scale bars in Figures 5d–5f are 0.5 m; green lines in Figures 5d and 5g are lasers 10 cm apart.

Figure S2a). One *ROPOS* ROV dive (R1010) crossed the western edge of this lava lobe in 2006, although it was not recognized as 1998 lava at the time (Figure 5c). Nevertheless, the ROV video shows older lineated and jumbled lava with sponges west of the contact and young uncolonized lavas east of it, consisting of a steep pillowed flow front rising to a gentler flow interior of lobate lavas (Figures 5d–5g). Therefore, we describe the map-scale morphology in Figure 5 as inflated lobate flows near the eruptive vents, and the western end of this flow as an inflated pillow flow, with a transition zone of channelized sheet flows in between (Figure 3a).

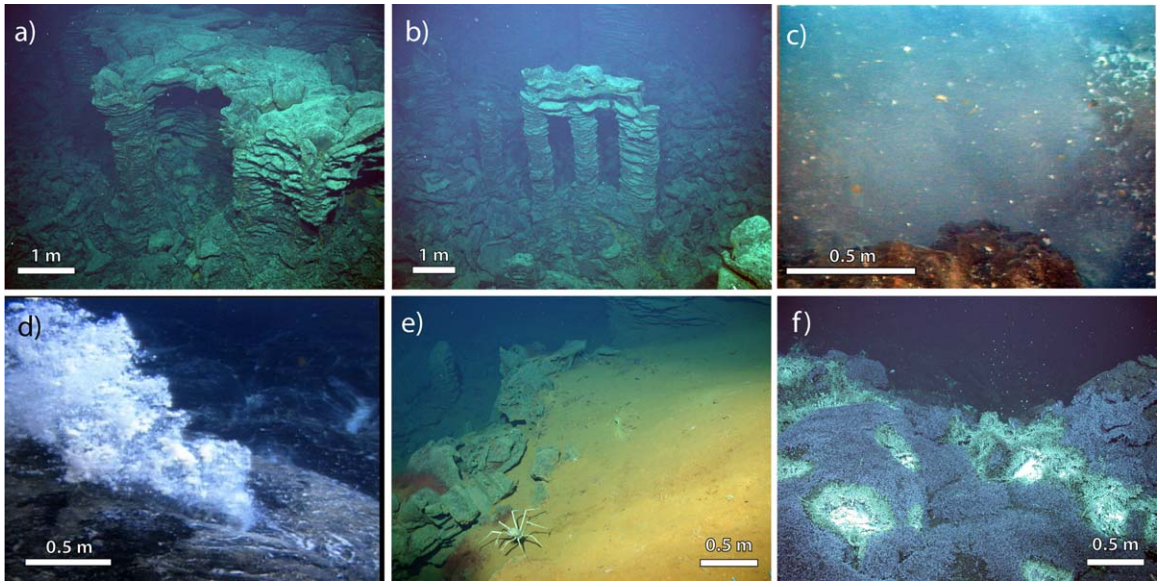

Figure 6. Photographs in the north part of the Northern 1998 lava flow (see Figure 5a for locations). (a and b) Lobate sheet flow with extensive collapse and remnant lava pillars near eruptive fissure C (*Jason* dive J2–291 in 2007). (c and d) Snowblower vents located within ~50 m of the eruptive fissures that were active after the eruption (Milky vent and The Pit; *ROPOS* dives R460 and R464 in 1998). (e) Heavy orange hydrothermal sediment found within ~50 m of parts of eruptive fissure C, (*Jason* dive J2–291 in 2007). (f) Marker N3 vent characterized by extensive blue mat of colonial protozoan ciliate (*Jason* dive J2–291 in 2007).

[20] The earliest ROV dives at the north end of the flow (August–September 1998) found several "snowblower" hydrothermal vents [*Haymon et al*., 1993; *Delaney et al*., 1998; *Embley and Lupton*, 2004], including vents named Magnesia, Ouzo, Easy, Milky, and Minisnow, all located within ~50 m of the eruptive fissures (Figures 5, 6c, and 6d). Almost all these snowblower vents cooled and died out within 1–2 years of the eruption, while other vent sites on the 1998 flow further south persisted [*Butterfield et al*., 2004; *Huber et al*., 2006; *Marcus et al*., 2009; *Opatkiewicz et al*., 2009]. Another distinctive feature of this area is the locally heavy accumulations of orange hydrothermal sediment that are only found within ~50 m of eruptive fissure C, but are not observed south of 45° 56.4′N (Figure 6e). Also unusual was the "Marker N3" diffuse vent site, which hosted a "blue mat," made up of a colonial protozoan ciliate [*Kouris et al*., 2007; *Kouris et al*., 2010] that covered most of the seafloor over an area of 300 m^2 (Figure 6f).

3.3.2. Middle Part of the Northern 1998 Lava Flow

[21] In contrast to the north end, the middle section of the Northern 1998 lava flow (45° 55.4′-56.5′N; erupted from fissures D and E) was relatively well-mapped soon after the event by dive observations of lava contacts and Imagenex bathymetry (Figure 3b). The middle section of the flow was much narrower in the E–W direction (300–600 m) than the northern end, because the seafloor is relatively flat in this area and the flow was restricted by topographic barriers (Figure 7). In addition, this area is near the buried edge of the caldera so the slope gradually increases in gradient from north to south, and consequently lava drained from the middle section southward (Figures 3a and 7; supporting information Figure S2).

[22] The middle section of the 1998 flow was an inflated lobate flow with collapse areas 2–3 m deep along its central axis. The photo-scale lava morphologies on this part of the 1998 flow were distributed in a very regular pattern. The thin (<1 m) margins of the flow were pillow lava (Figure 8a). Where the flow was thicker (> 1 m), the lava morphology was lobate (Figure 8b); this was the appearance of most uncollapsed parts of the flow. Near the edge of collapse areas, the lobate upper crust was commonly hollow underneath where the molten interior of the flow had drained out, and lava pillars were exposed (Figure 8c). In the floor of the collapses, there were various sheet lava morphologies including lineated (Figure 8d), ropy, whorled, and jumbled (Figure 8e).

[23] We have unique information on the dynamics of the 1998 eruption in this area from an instrument that was caught in the lava flow ("VSM2" in Figure 7). It had a pressure sensor that showed that the instrument was uplifted by ~3 m in only one

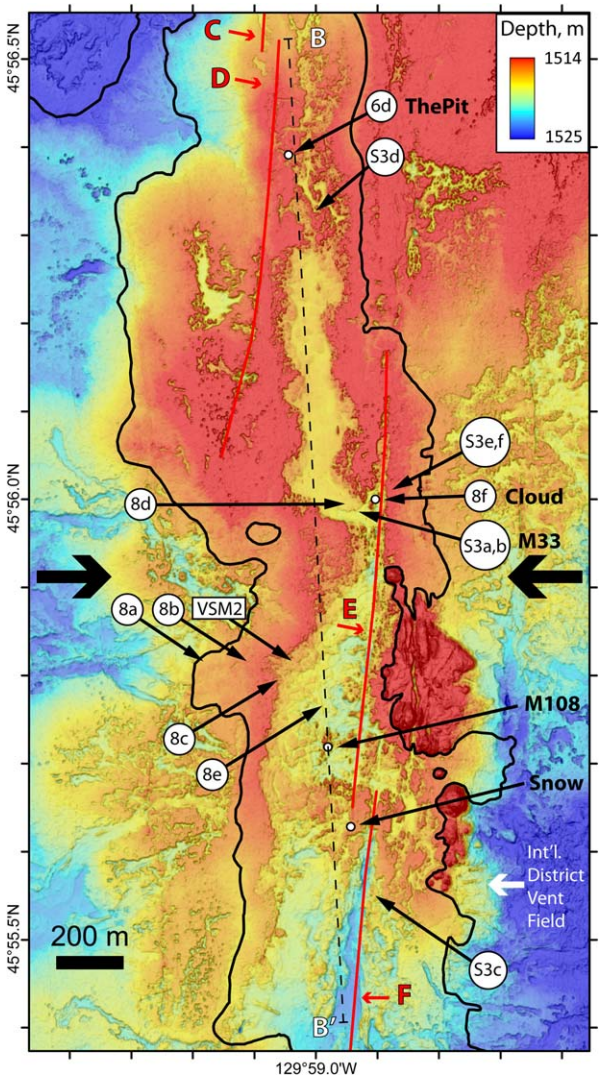

Figure 7. AUV bathymetric map of the middle section of the Northern 1998 lava flow (black outline; see Figure 3a for location; red lines are eruptive fissures C-F). Dashed line B–B′ is depth profile in supporting information Figure S2b. Bold black arrows point to topographic constriction discussed in the text. White dots are snowblower vents, including The Pit, Cloud, Marker 108 (M108), and Snow (labeled). Marker 33 vent (M33) is located 80 m WSW of Cloud vent. International District vent field in lower right includes high-temperature sulfide and anhydrite chimneys. Circled numbers show locations of images in Figures 6, 8, and S3. VSM2 is instrument that was caught in lava flow.

hour while the lava flow inflated and then gradually lowered again as the lava flow drained out during the next hour and a half [*Fox et al.*, 2001]. This showed that the emplacement of the 1998 lava flow (at this location) was relatively rapid and only lasted 2.5 h. The lava first flowed under the instrument, which became embedded in the upper crust of the flow, then was lifted as the flow inflated, and finally it was set back down during lava drain-out (see supporting information Animation S1). Only 1 m of lava remained in the floor of the collapse after drain-out. This unique data set gave new insights into the process of lava flow inflation on the seafloor and the formation of lava pillars during the emplacement of lobate flows [*Gregg and Chadwick*, 1996; *Chadwick*, 2003]. Depth profiles suggest the middle section of the 1998 lava flow likely inflated up to a maximum thickness of ~5 m before it drained (supporting information Figure S2b). This is the only place where we have a firm constraint on the duration of lava emplacement, and although it may have been longer elsewhere, we interpret from the flow morphology that the eruption duration was probably hours rather than days.

[24] Near 45° 55.9′N, there was apparently a topographic constriction (arrows in Figure 7) that caused lava to pond to the north before it drained to the south. The constriction was due in part to the older, high-standing, fractured mound of pillow lava that lies to the east of the flow (east of the VSM2 instrument in Figure 7), possibly a remnant of the older (mostly buried) caldera rim. This probably explains why the flow north of this point is mostly intact with only 19% of its area collapsed, whereas to the south the percentage increases to >50%. The constriction limited how quickly lava that was erupted to the north could drain to the south, thus limiting the amount of collapse, whereas there was no such check on the rate of lava drain-out to the south. The N-S slope also increases from ~0° north of the constriction to ~0.5° south of it (supporting information Figure S2b). This also explains why the prominent collapse area between eruptive fissures D and E north of the constriction is floored by flat lineated sheet flows (evidence of ponded flow conditions during gradual lava drain-out; *Chadwick et al.* [1999a]), whereas to the south the floor of the collapses becomes dominated by jumbled lava morphology with fewer lava pillars. Likewise, the morphology of the eruptive fissures changes north and south of the constriction. To the north, the eruptive fissures are marked by narrow linear collapses along their lengths; to the south, they appear as deep linear clefts in the floors of the collapse areas (Figure 7).

[25] Temporal changes in the surficial appearance of the lavas in the middle section of the flow were documented by submersible and ROV dives between 1998 and 2011. Immediately after the 1998 eruption, where the 1998 lavas were thicker

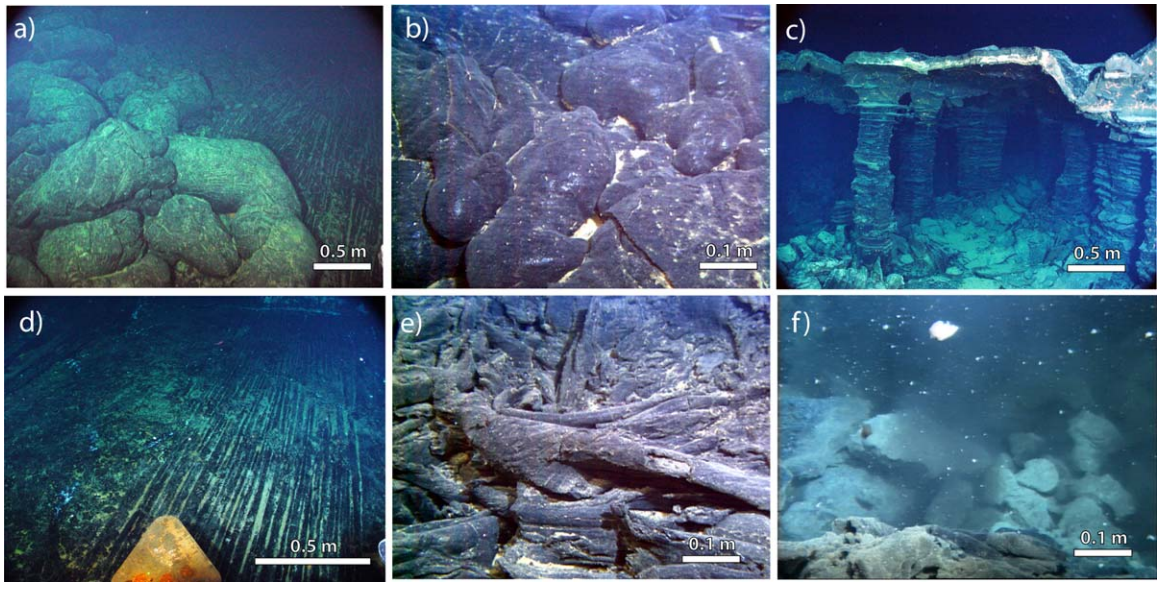

Figure 8. Photographs in the middle part of the Northern 1998 lava flow (see Figure 7 for locations). (a) Pillows of 1998 lava over older seafloor along the margin of the flow (*ROPOS* dive R1012 in 2006). (b) Lobate morphology is found on all uncollapsed parts of the flow where it is >1–2 m thick (*ROPOS* dive R493 in 1999). (c) Edge of the central collapse area, looking back at the uncollapsed lobate crust supported by lava pillars (*ROPOS* dive R743 in 2003). (d) Lineated sheet flow in the floor of the collapse area north of the constriction shown in Figure 7 (*ROPOS* dive R1010 in 2006). (e) Jumbled sheet flow in the floor of the collapse area south of the constriction (*ROPOS* dive R492 in 1999). (f) Cloud snowblower vent near eruptive fissure E (*ROPOS* dive R460 in 1998).

than ~2 m, the lavas were almost completely covered with a fuzzy white to tan colored mat (supporting information Figure S3). This "eruption mat" was most evident on areas of inflated lobate lavas, but was also observed within adjacent collapse areas. The mat was white in areas that were still actively cooling or venting (supporting information Figures S3a and S3b), and scaleworms and limpets actively grazed the white mats [*Marcus and Hourdez*, 2002; *Marcus et al*., 2009]. Where cooling-related venting had waned, the mat was tan and without grazers. Around some point-source hydrothermal vents, a concentric pattern was observed with white mat growing nearest the orifice, surrounded by tan mat (supporting information Figure S3c). Initially, the tan mat was confusing, because it looked like pelagic sediment causing the newly erupted lavas to appear much older. However, on close examination the mat was clearly not sedimentary in origin because it covered vertical and even overhanging surfaces (supporting information Figure S3d) and had a filamentous texture (supporting information Figures S3e and S3f). In contrast, the thin, pillowed margins of the flow were not covered with the mat. We suggest that this "eruption mat" is microbial in origin and grows in place during the post-eruption cooling phase of a newly emplaced lava flow, but only on inflated lobate lavas that are thick enough to retain their heat and cool over an extended period of time (perhaps weeks to months). The mat gradually degraded and disappeared over the first few years after the 1998 eruption. A similar "eruption mat" was observed again on thick (>2 m), inflated lobate flows erupted in April 2011 at Axial Seamount [*Meyer et al*., 2013]. This "eruption mat" is distinct from other microbial mats that only form around active hydrothermal vents [*Juniper et al*., 1995; *Moyer and Engebretson*, 2002; *Emerson and Moyer*, 2010; *Meyer et al*., 2013], because it formed directly on the new lava surface in the absence of focused hydrothermal fluids.

[26] Similar to what was observed at the north end of the 1998 lava flow, snowblower vents in the middle section were located within ~50 m of the eruptive fissures (and the underlying feeder dikes), including vents named The Pit, Snow, Minisnow, and Cloud vent (Figure 7). Cloud vent (Figure 8f) was the largest and longest-lived snowblower vent after the 1998 eruption, but declined in temperature and vigor between 1998 and 2010 [*Baker et al*., 2004]. In contrast, Marker 33 vent, a nearby diffuse low-temperature vent, also declined in temperature after the eruption but reached a steady state and continued to be active, supporting a diverse vent biological community until the 2011

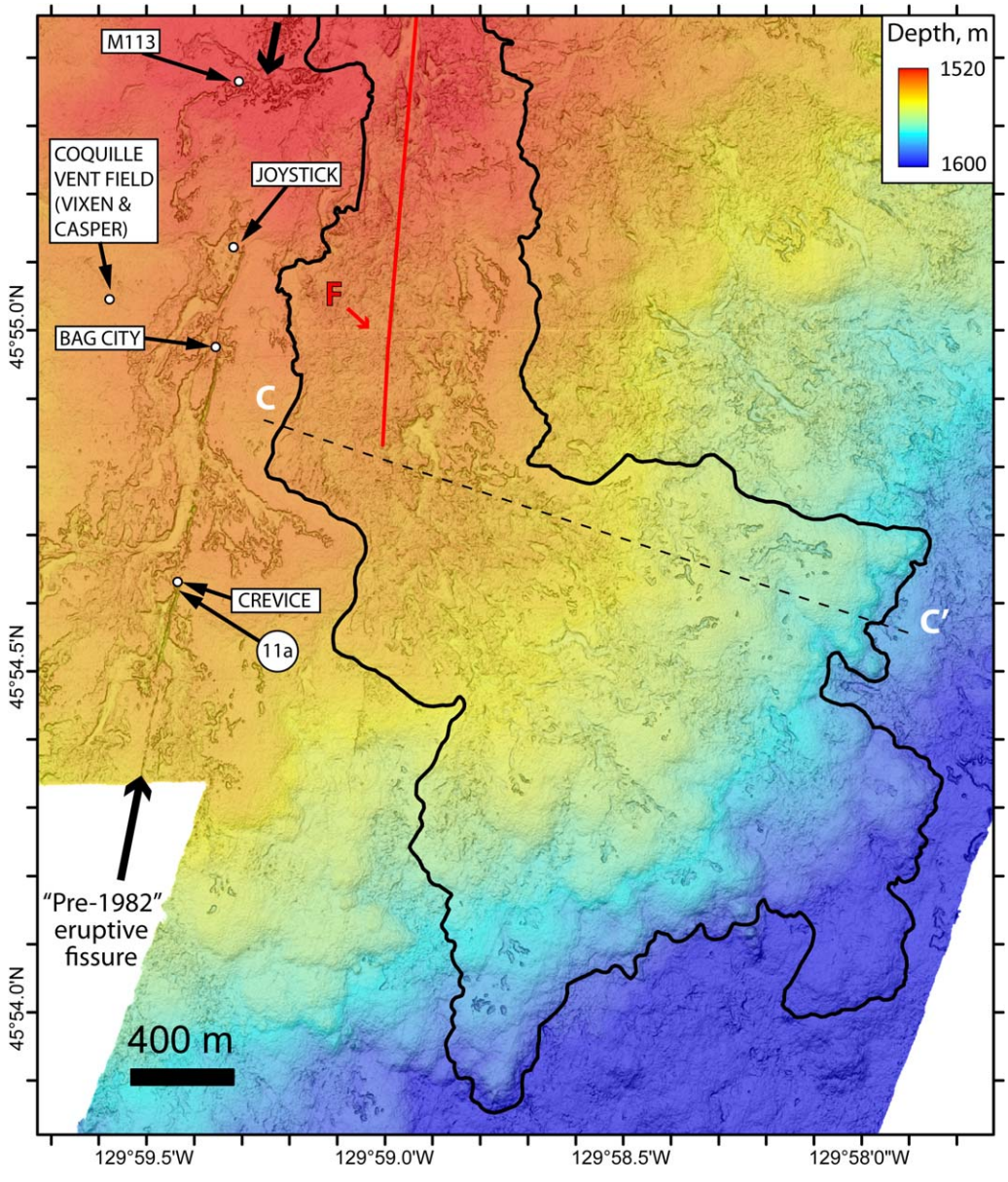

Figure 9. AUV bathymetric map of the south part of the Northern 1998 lava flow (black outline; see Figure 3a). 1998 lava morphology is mostly jumbled in the upper half of the area where lava drained southward from the north, and mostly inflated pillow flows at the distal end. White dots are hydrothermal vents, including Marker 113 (named Axial Gardens in *Embley et al*. [1990]), Joystick, Bag City, and Crevice (all located along the "pre-1982" eruptive fissure, discussed in text and denoted by large black arrows). Coquille vent field (including Casper/Vixen vents) is located west of the "pre-1982" lava flow on older lava. Dashed line C–C′ is depth profile in Figure S4a.

eruption [*Huber et al*., 2003; *Butterfield et al*., 2004; *Huber et al*., 2006; *Marcus et al*., 2009].

[27] Submersible dives and camera tows before the 1998 eruption documented diffuse hydrothermal vents in this area [*Embley et al*., 1990], some with dense tubeworm communities. Many of these pre-existing vent communities were buried during the eruption, but remarkably, new diffuse vents appeared on the new lava flow in approximately the same locations (e.g., Marker 33 vent). Thus, the diffuse vents along the upper south rift zone at Axial appear to be persistent features, apparently controlled by deep rift structures that have a strong influence on the subsurface hydrothermal circulation patterns, but which are not disrupted by individual dike intrusions [*Butterfield et al*., 2004]. This is in strong contrast with the snowblower vents, which seem to mine the available heat from

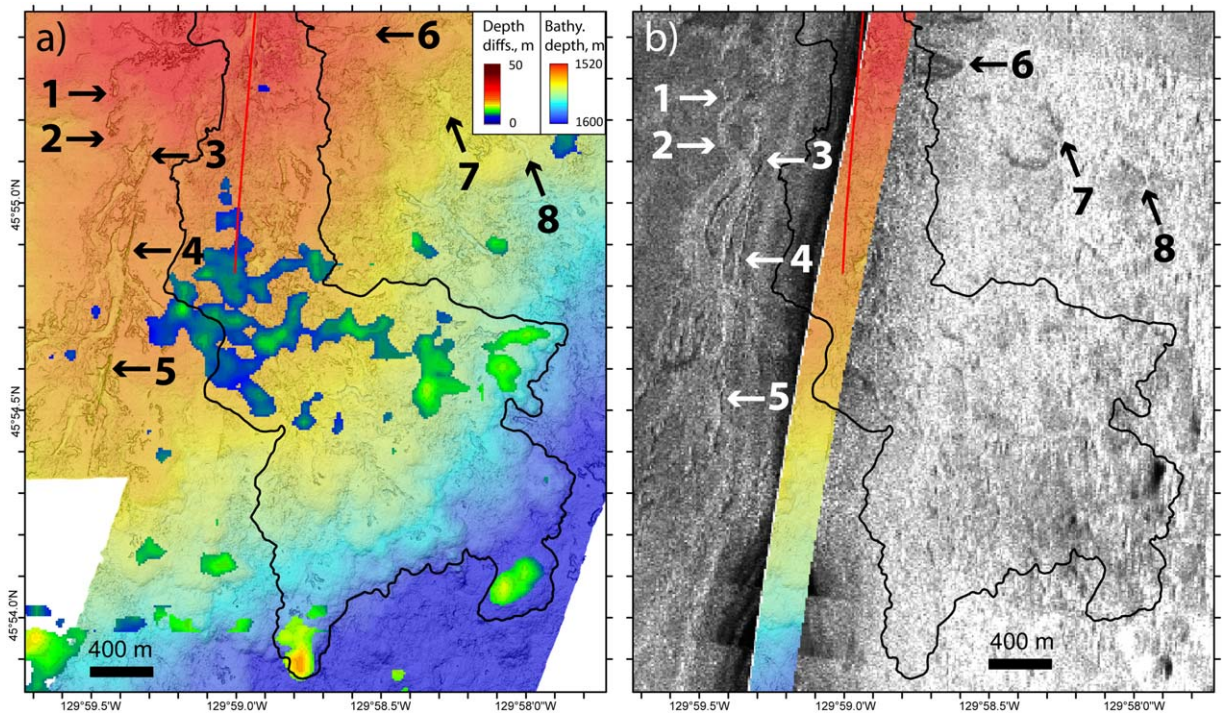

Figure 10. Maps of the south part of the Northern 1998 lava flow (black outline). Numbers and arrows show corresponding features in Figures 10a and 10b. (a) Largest ship-based multibeam depth changes [from *Embley et al*. 1999] correspond with distal lobes of the flow. (b) Sidescan data (5 km swath) shows that eruptive fissures, lava channels, and collapse features just to the west of the 1998 lava flow were in place in 1986, despite being almost indistinguishable in age. Unfortunately, there are no prominent features in the sidescan imagery within the 1998 lava flow outline that are clearly buried by 1998 lava, as in Figures 4 and 5.

the feeder dikes within a year or two following an eruption and then expire [*Crowell et al*., 2008].

[28] A vent field of high-temperature sulfide and anhydrite chimneys called the International District is located east of the 1998 flow at 45° 55.57′N, 129°58.77′W (Figure 7). This field was discovered after the eruption, but almost certainly predates it based on the number of large sulfide chimneys. This vent field was topographically shielded from the 1998 lavas by a north-south row of older pillow-lava mounds that may have erupted along the (mostly-buried) caldera-bounding fault (Figure 7).

3.3.3. South Part of the Northern 1998 Lava Flow

[29] The south end of the Northern 1998 lava flow (south of 45° 55.4′N) was fed from eruptive fissure F and from southward drain-out of lava erupted from fissures D and E in the middle section of the flow (Figure 9). This part of the flow crosses the presumed location of the buried caldera rim (Figure 1b) and follows an increase in slope from 1 to 5° to the south-southeast toward its distal end at ∼1640 m (supporting information Figure S4). The south end of the flow has much sparser dive coverage than the middle section. Consequently, the flow boundaries are mapped by visual observations where available (Figure 3b) and otherwise are interpreted from the AUV bathymetry (particularly at the distal end where pre-1998 sidescan imagery is not useful for mapping the extent of 1998 lava; Figure 10).

[30] The lava morphology here is mostly channelized jumbled lava within broad areas of collapse and lava drain-out, except near the distal end of the flow. The distal 300–500 m of the flow is mostly uncollapsed, inflated pillow flows, typically 200–500 m wide and 5–10 m thick (Figure 9). Some of these inflated pillow flows have narrow, branching, locally dendritic collapses in their cores, exposing parts of their internal lava feeder system, again similar to skylights over lava tubes on land, or marking the extent of their molten cores. Because of the regional slope to the southeast, the western contact of the 1998 lava is shallower than the eastern contact and laps up on preexisting topography. In contrast, the eastern edge of the flow appears more like a flow front or levee with a 100 m wide rim of intact uncollapsed pillow lavas (Figure 9). From this distribution of lava

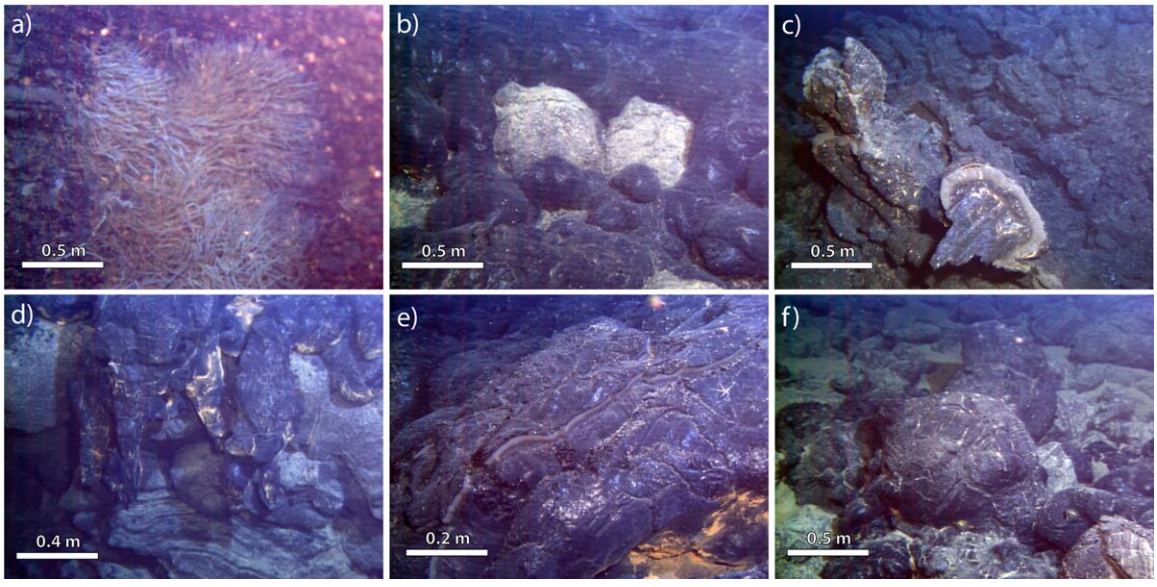

Figure 11. Images on and near Southern 1998 lava flows G-I and J. (a) Mature tubeworm bushes at Crevice vent, evidence that the "pre-1982" eruptive fissure shown in Figure 9 was not active during the 1998 eruption. (b) Contact at NE edge of 1998 Flow G–I. (c) Jumbled lava in middle of Flow G–I on 4° slope. (d) Lava pouring into older collapse at edge of Flow G–I. (e) Close-up of 1998 lava at same location. (f) Pillow lava at western contact of Flow J. Images from *ROPOS* dives R494 and R495 in 1999. Photo locations shown in Figures 9 and 12.

morphologies, we interpret that as the lava flowed downslope it initially inflated into broad lobes with a solid upper crust and fluid interior, but as the fluid lava continued to drain downslope, the upper crusts on upslope parts of the flow collapsed, either partially or extensively, depending on the degree of drain-out. Because of this, a large part of the interior of the flow has jumbled lava morphology (channelized, drained-out lava). The distal flow front was the last to form and inflate, and so it is uncollapsed, because much of the lava that drained from the upslope parts of the flow ended up there. The pre-eruption and post-eruption ship-based multibeam comparison [*Embley et al*., 1999], while sparse and noisy, is consistent with our mapped flow boundary because it shows the greatest depth changes near the inflated pillow flows at the distal end (Figure 10a).

[31] No active hydrothermal venting was observed on the south end of the Northern 1998 lava flow, but there were few dive observations there. The (apparent) lack of venting may be because much of the flow was not underlain by a feeder dike and was relatively thin (having drained downslope from the north). In contrast, there were numerous hydrothermal vents within 500 m west of the western contact of the 1998 lava flow in this area. These vents included Marker 113 vent (known before the 1998 eruption as "Axial Gardens"; *Embley et al*. [1990]), Joystick, Bag City, and Crevice vents, all aligned along a previous eruptive fissure that is clear in the AUV bathymetry (Figures 9 and 10). All of these vent sites had mature tubeworm communities when visited by ROV in 1998–1999, clear evidence that the 1998 eruption did not inundate this area (Figure 11a). This older eruptive fissure fed a lava flow that drained to the south-southwest with braided channels and collapses that parallel the fissure on both sides. This flow (identified as Flow "Sa" in *Clague et al*. [2013]) is "pre-1982" because the earliest pre-eruption sidescan imagery shows that it was already in place (Figure 10b), yet it had a youthful appearance and was visually almost indistinguishable from 1998 lava (glassy, with little sediment, and no sessile organisms). Though not used in 1998, this "pre-1982" eruptive fissure was reactivated during the 2011 eruption [*Caress et al*., 2012]. Another major hydrothermal vent field called Coquille (because of abundant clams) is located 300 m west of Bag City vent (Figure 9) on a lava surface that is older still (less glassy, more sediment, and covered with sessile organisms). The Coquille vent field is about 100 m across, is characterized by diffuse venting with numerous tubeworm bushes, and also hosts two high-temperature anhydrite chimneys called Vixen and Casper, both venting fluid ~300°C and

located only 10 m apart. All the high-temperature anhydrite chimneys known at Axial (Virgin, Vixen, Casper, Castle, Diva, and Trevi) are located near the exposed or presumed-buried caldera fault (Figure 1b). Their high-gas, low-metal contents are thought to result from phase separation at depth as fluids rise along the caldera fault [*Butterfield et al*., 1990].

3.4. The Southern 1998 Lava Flows

[32] As noted earlier, there were three separate but closely spaced Southern 1998 lava flows that we distinguish by their eruptive fissure names: Flow G–I, Flow J, and Flow K (Figure 3a). The five eruptive fissures that fed them were all aligned and are connected by open cracks (Figure 12). Fissure G, the northern-most of the three eruptive fissures that fed Flow G–I, was located at the south end of the "pre-1982" fissure, discussed above, which was reused during the 2011 eruption [*Caress et al*., 2012]. Flow G–I has inflated lobate flow morphology near the eruptive vents (Figure 11b), which transitions to channelized jumbled lava on the steep (3.5°) eastern flank of the rift zone (Figure 11c), and turns into inflated pillow flow morphology at the flow terminus ~1 km from the vents (Figure 12). Near fissure H, 1998 lava poured into pre-existing collapse pits (Figures 11d, 11e, and 12). Flow J was the smallest and had thin pillowed margins (Figure 11f) and a thicker lobate interior with collapse areas (Figure 12). Near its eastern margin, Flow J flooded and filled a 15 m wide pre-existing fissure that subsequently drained toward the SE while the lava was still molten, leaving bathtub ring structures coating the sides of the fissure. The south end of Flow G–I partially fills the same fissure. This shows that young fluid lava flows do not always completely bury pre-existing topography and in fact sometimes mimic it, as was shown by Axial's 2011 eruption [*Caress et al*., 2012].

[33] Flow K, the largest and southern-most of the three Southern 1998 lava flows (Figure 13a) spans depths between 1700 and 1800 m, considerably deeper than the rest, was emplaced on the steepest slope (4°), and is also the thickest 1998 flow (supporting information Figure S4b). It was discovered soon after the 1998 eruption because it is 10 m thick at its upslope end and 26 m thick at its eastern downslope end (Figure 13b), and consequently produced a robust depth change in the ship-based multibeam resurvey [*Embley et al*., 1999]. It was mapped by a combination of ship-based multibeam, AUV multibeam, and dive observations (Figure 3b). The eruptive fissure that fed Flow K is 1.4 km long oriented at 015°, parallel to many surrounding older fissures that are visible in the AUV bathymetry along the rift zone (Figure 13a).

[34] At the south end of eruptive fissure K, 1998 lava can be seen coming directly out of an open crack (the top of the dike). Where unburied, the fissure is 1.5 m wide, which presumably represents the width of the 1998 dike and the amount of seafloor spreading that occurred during this eruption (at this location). From south to north, dive observations along the fissure follow a progression from 1998 lava visible inside and filling the crack several meters below the rim (Figure 14a), further north the level of 1998 lava gets higher in the crack (Figure 14b), until it overflows the fissure (Figure 14c), and finally buries it completely under pillow lava (Figure 14d). At the northern end of eruptive fissure K, the 1998 lavas form a low ridge of pillow and lobate lavas, 100–200 m wide (northern area labeled "1" on Figure 15). On the eastern edge of this ridge, 1998 lobate lavas flowed downslope, partially filled an older eruptive fissure, and subsequently formed drain-out structures along its length (Figure 14e). Drain-out structures were also observed in the walls of collapse pits within the main body of the flow, evidence that it once had a molten core (Figure 14f).

[35] The majority of the lava in Flow K was fed from the center of the eruptive fissure. From there, lava extended downslope to the east in a stair-step morphology of alternating steep flow fronts and flatter sections (Figure 13a; supporting information Figure S4b). The north-south width of the flow was 300–400 m, largely constrained by previous topography. Observations during *ROPOS* dive R465 showed how the lava morphology changed along an E-W transect (Figure 13c). The eastern steep flow front was all pillow lava (supporting information Figure S5a), and above that it transitioned to broad lobate flows (supporting information Figure S5b), and the pattern repeated upslope (supporting information Figure S5d) with steep pillowed flow fronts alternating with flatter lobate sections, some with collapse areas 5–10 m deep with lava drain-out bathtub rings on the walls (supporting information Figure S5c). In the floor of the upper collapse were jumbled (supporting information Figure S5e) to ropy lava (supporting information Figure S5f), with lobate lava again on the edges of the largest collapse area (supporting information Figure S5g), and finally pillow lava once more at the western flow margin (supporting information Figure S5h). No active hydrothermal

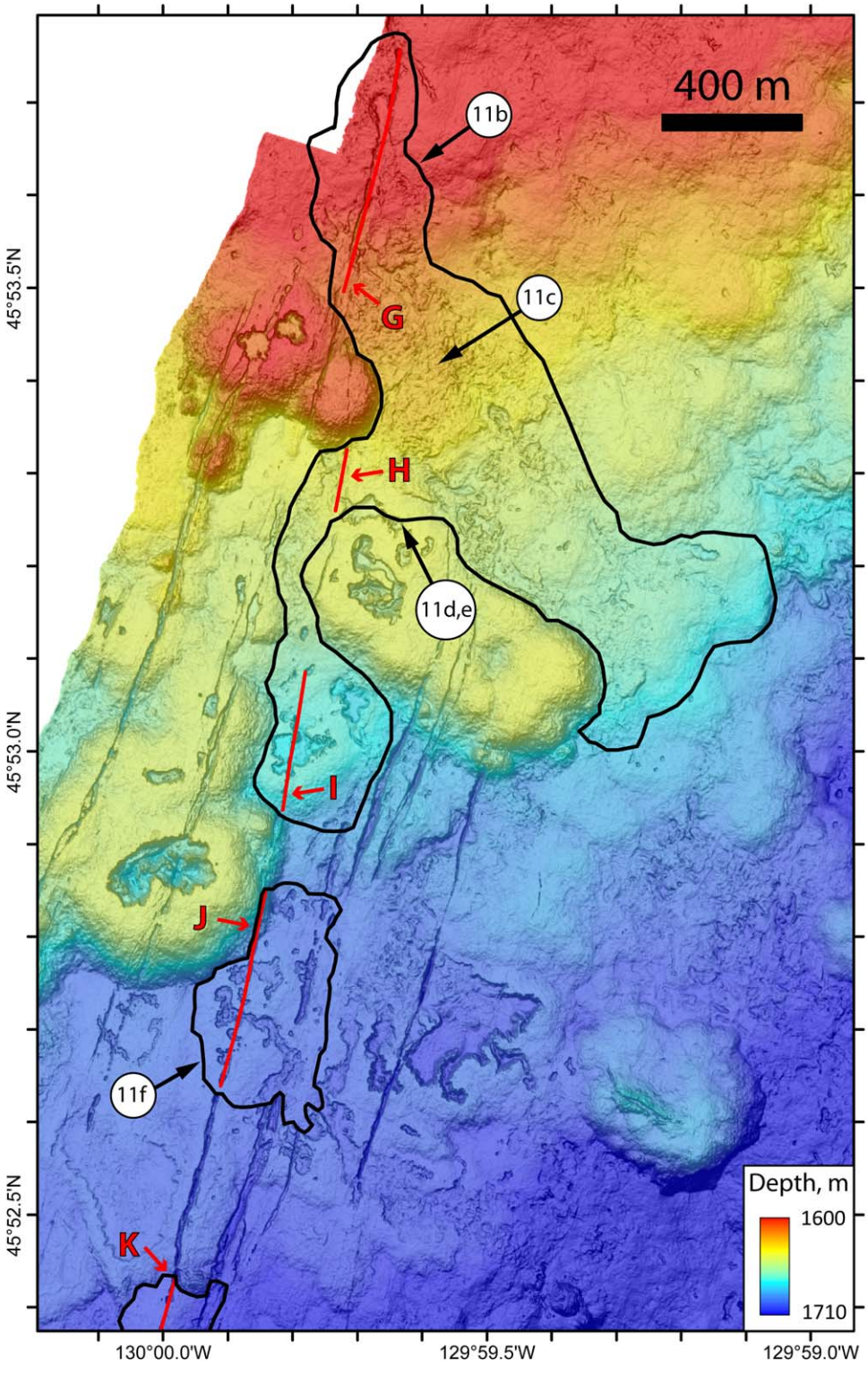

Figure 12. Map of Southern lava flows G–I and J (black outlines; see Figure 3a). Eruptive fissures G–K (red lines) and locations of images in Figure 11 are shown.

venting was observed on the Southern 1998 flow, even though the first dive observations were made in August 1998, probably because most of the flow is comprised of pillow lavas that are permeable and were therefore quickly cooled. Being on the rift zone, it is also south of the caldera and its

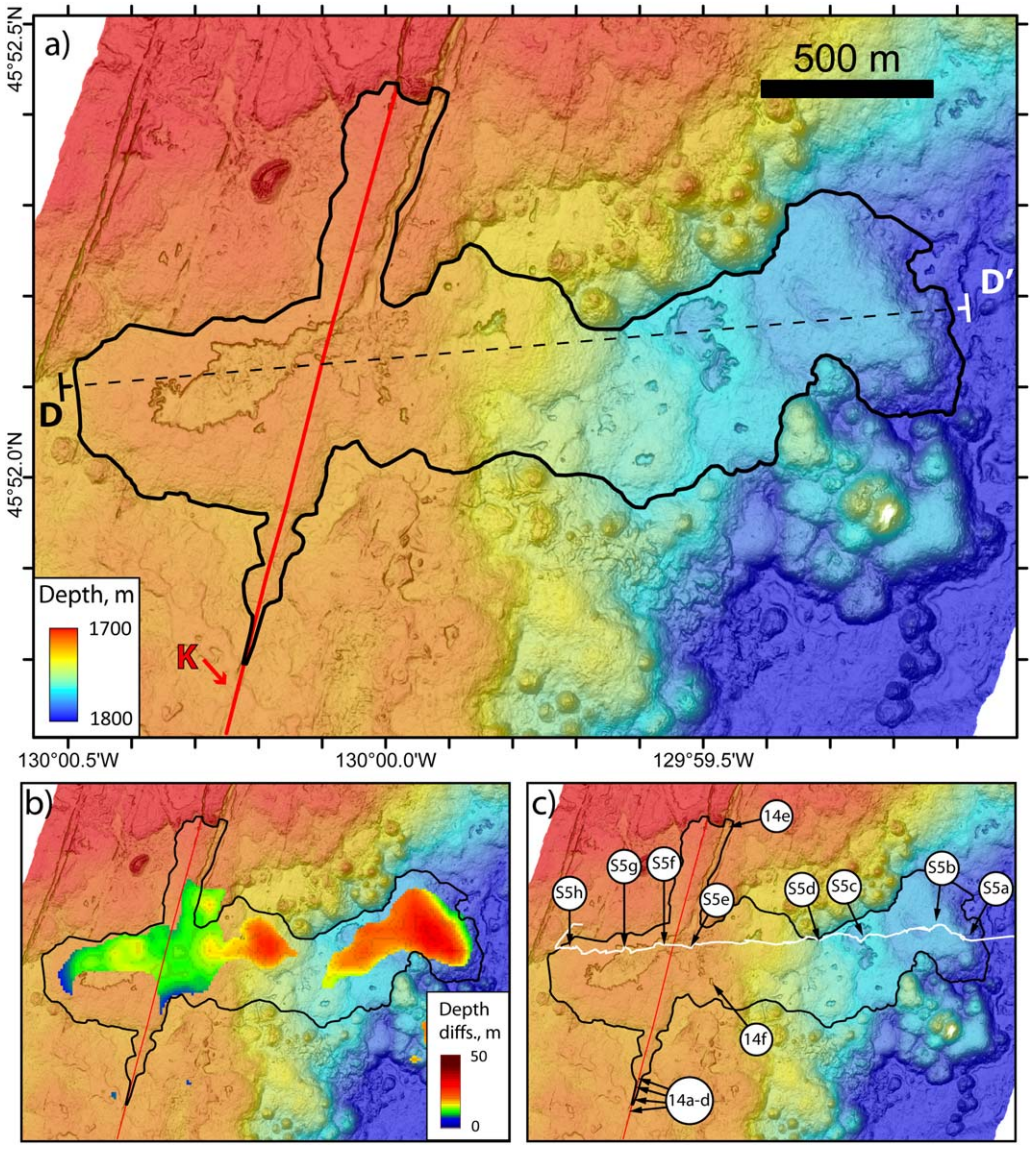

Figure 13. Map of the Southern 1998 lava flow K (see location on Figure 3a). (a) AUV high-resolution bathymetry with 1998 lava flow (black outline) and eruptive fissure K (red line). Dashed line D–D′ is depth profile in supporting information Figure S4b. (b) Ship-based multibeam depth differences between 1981–1991 [from *Embley et al*. 1999] overlain on bathymetry. (c) Locations of images in Figure 14 and supporting information Figure S5 along ROV dive track R465 (white), and from dives R554 and J2–289 (not shown).

underlying magma reservoir [*West et al*., 2001; *Kent et al*., 2003].

[36] We interpret a sequence of events during the emplacement of Flow K as follows. Lava initially erupted along all of eruptive fissure K and formed the low pillow ridges (labeled "1" in Figure 15a), which partially dammed a large lobe of more fluid lava that ponded to the west of the fissure (labeled "2" in Figure 15a) before lava drained through a narrow outlet and flowed 1.3 km downslope to the east. To the east, lava lobes were emplaced that were successively shorter as the eruption rate waned, forming a shingled arrangement (labeled "3–6" in Figure 15b), as evidenced by the upslope sides of collapse areas being partly buried from above (Figures 15c and 15d). Simultaneously, the lava drained out of the western inflated, ponded lobe and created the large collapse area in its core. This sequence of events produced a lava flow with characteristics of an inflated lobate flow near the eruptive vents and an inflated pillow flow downslope (Figure 3a).

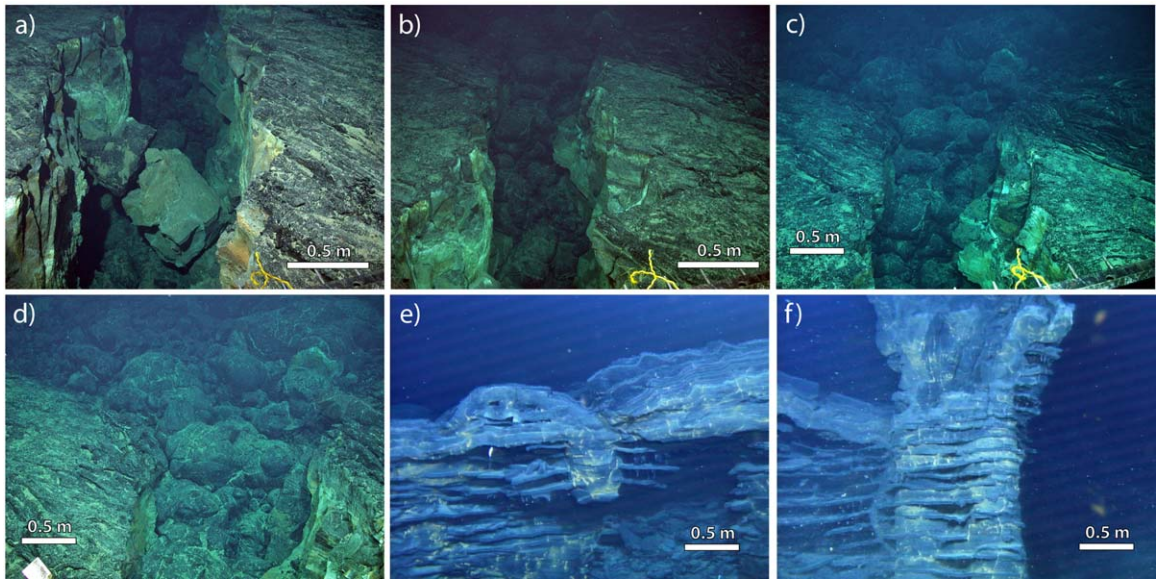

Figure 14. Images from the Southern 1998 lava flow K, (a–d) along the eruptive fissure at the south end (views facing NNE) and (e–f) inside collapses (see Figure 13 for image locations). (a) Dark 1998 pillow lava fills the 1.5 m wide eruptive fissure ~2 m below fissure rim. Light colored block at center has fallen into fissure from western fissure wall. (b) About 5 m further north, dark 1998 pillow lava rises up to the depth of the fissure rim (in the distance). (c) Another 5 m further north, dark 1998 pillow lava overflows the eruptive fissure. (d) Dark 1998 pillow lava flows out over the seafloor on either side of the eruptive fissure. (e) 1998 lava coats the wall of a preexisting fissure where it filled and then drained out. (f) View from inside a collapse pit showing lava drain-out structures covering the walls, evidence that the flow had a molten core. Figures 14a–14d from *Jason* dive J2–289 in 2007, Figures 14e–14f from *ROPOS* dive R554 in 2000.

4. Discussion

4.1. Relationships Between Map-Scale Submarine Lava Flow Morphologies

[37] The high-resolution AUV bathymetry of the 1998 lava flows provides one of the first comprehensive and detailed views of the map-scale flow morphology of newly erupted submarine lava flows. Such a view is difficult to deduce from photo-scale mapping alone. From this data set, we interpret that there is a continuum in map-scale flow morphologies between "inflated lobate flows" and "inflated pillow flows," locally with channelized sheet flows in between (Figure 3a). We interpret that "pillow mounds and ridges" are a separate map-scale flow morphology that are produced by lower effusion-rate eruptions [*Yeo et al*., 2013]. Below, we discuss these terms in the context of the 1998 lava flows and our interpretation of their emplacement.

[38] "Inflated lobate flows" are exemplified by the middle section of the Northern 1998 lava flow. They are formed by lava erupted in relatively flat terrain or within enclosed basins. They have flat tops with a lobate morphology, and have thin pillowed margins where they form their own flow fronts, or the lobate lava may extend to the edge of the flow where it laps up against previous topography (for example, the eastern contact, east of the VSM2 instrument in Figure 7). They reflect a relatively high effusion rate when lava is being supplied faster than it can be carried away, and consequently inflated lobate flows are a near-vent flow morphology, meaning they form within a few hundred meters of eruptive vents. A key characteristic of these flows is that they have a molten, hydraulically connected interior (Figure 2a). They initially spread out as thin sheets, undergo flow inflation [*Gregg and Chadwick*, 1996], and then may drain out, forming collapse areas in the central parts of the flows that expose lava pillars supporting remnants of the upper lobate crust (Figure 2a and supporting information Animation S1). Other sheet lava morphologies in the 1998 flows, such as lineated, ropy, and jumbled, formed during drain-out and are exposed in the floors of collapse areas, always channelized within the pillowed or lobate margins of the flow. At Axial, the inflated lobate flows are typically 5–10 m thick (when fully inflated) and their collapse areas are 2–5 m deep. On slopes, lobate sheet flows inflate quickly

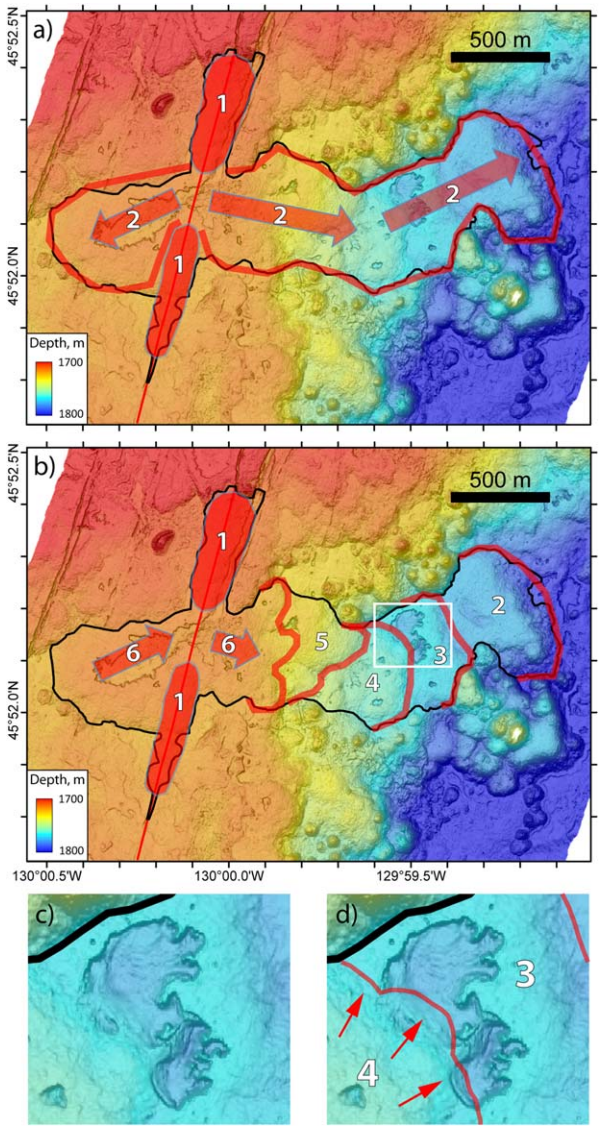

Figure 15. Maps showing interpretive sequence of events during emplacement of the Southern 1998 lava flow. (a) A ridge of pillow and lobate lavas was constructed along the ends of the eruptive fissure (#1), which partially dammed a lobe of lava that flowed to the west, at the same time that lavas flowed downhill to the east from the central part of the fissure (#2). (b) Lobes #2–6 were emplaced in a shingled sequence (from longest to shortest), as evidenced by the upslope flow fronts overlapping downslope drain-out features, such as between lobes #3 and #4 (c and d).

and drain-out downslope just as quickly, leaving areas of extensive collapse and channelized jumbled lava (like at the north and south ends of the Northern 1998 flow). Thus, the extent of collapse depends strongly on the underlying slope and the amount and rate of lava drain out.

[39] "Inflated pillow flows" (Figure 2b) are a distinct map-scale flow morphology that formed during the 1998 eruption at Axial at the distal ends of "inflated lobate flows," where lava flowed downslope at least 0.5–1.0 km from the eruptive vents (Figure 3a). They are typically 10–30 m thick, are domed in profile, and are mainly pillows on their steep margins with lobate lava in their interiors. These flows also have molten cores that inflate and may drain-out downslope to form finger-like or dendritic collapse areas, but the cores are smaller than in inflated lobate flows, and lava pillars are rare or absent (Figure 2b). The interiors of collapse areas are coated with drain-out structures (horizontal bathtub-ring-like shelves) and the floors are commonly covered with jumbled lava. On the other hand, where they form at the downslope ends of flows, they inflate without subsequently collapsing (like the distal flow lobes at the north and south ends of the Northern 1998 flow, or many parts of the 2011 lava flows erupted within Axial caldera [*Caress et al*., 2012]).

[40] "Inflated pillow flows" have not been described in detail before, probably because they are best discernable with full-coverage, 1 m resolution bathymetry, and such data are still relatively rare. Photo-scale observations alone do not provide a large enough field of view nor a large enough spatial context to visualize and understand the topographic details of features that are hundreds of meters across. Nevertheless, high-resolution mapping of the rest of Axial caldera [*Clague et al*., 2013] and descriptions from other recent eruption sites [*Soule et al*., 2007; *Fundis et al*., 2010] suggest that inflated pillow flows are common features produced by high-effusion-rate eruptions and play an important role in the construction of the ocean crust.

[41] In contrast, we interpret that a third map-scale flow morphology, "pillow mounds or ridges" (Figure 2c), forms only during low-effusion-rate eruptions [*Gregg and Fink*, 1995]. This type is exemplified by the lavas erupted at 45° 41′N on the south rift zone during the 2011 eruption at Axial [*Caress et al*., 2012], the mid-1980s eruption at the northern Cleft segment [*Chadwick and Embley*, 1994; *Yeo et al*., 2013], or at various locations on the East Pacific Rise [*Perfit et al*., 1994; *White et al*., 2000; *Sinton et al*., 2002; *Escartin et al*., 2007; *White et al*., 2009]. Such flows are composed almost exclusively of pillows that pile up over the eruptive fissure. They form thick and steep-sided mounds and ridges, 20–200 m high, because the lava is not able to flow far from the eruptive vent. Key characteristics are that these

flows do not have a large molten hydraulic core, they do not inflate and drain-out, and they do not have collapse areas. Pillow mounds and ridges can be hummocky along their length if the eruption became localized along the eruptive fissure.

4.2. Estimates of Eruption Rate for the 1998 Lava Flows

[42] We can only place crude constraints on the eruption rate that fed the 1998 lava flows at Axial. The Northern 1998 lava flow had a volume of 22 $\times$ 10^6 m^3 (Table 1). We also know from the VSM2 instrument that was stuck in lava that the flow inflated and drained out in 2.5 h at its location. This provides a minimum eruption duration, but lava effusion could have lasted longer from other parts of eruptive fissures A–F, yet probably not more than 12 h, because no indications of vent-localization are observed [*Bruce and Huppert*, 1989; *Wylie et al*., 1999]. The volume of the Northern 1998 flow divided by these estimated minimum and maximum eruption durations yield an average lava discharge rate of 1.8–8.8 $\times$ 10^6 m^3/h (0.5–2.4 $\times$ 10^3 m^3/s). We think the lower end of this range is probably more realistic. For comparison, this is the same order of magnitude as rates of 1–2 $\times$ 10^6 m^3/h observed during the first days of the 1975 and 1984 eruptions of Mauna Loa volcano, Hawaii [*Lockwood et al*., 1987] or during the high-fountaining episodes of the Pu'u O'o eruption at Kilauea volcano, Hawaii [*Heliker and Mattox*, 2003], and is typical of other short-lived Hawaiian eruptions [*Wadge*, 1981]. It is also similar to the eruption rates calculated by *Soule et al*. [2005] for the flows that formed channel systems on the flanks of the East Pacific Rise at 9–10°N. This qualitatively confirms the impression from the lava flow morphology that this part of the 1998 Axial eruption was brief and intense. If we assume the same range of possible eruption durations for the southern-most 1998 lava flow (Flow K) and the lava volume in Table 1, the lava discharge rate would be 0.6–2.8 $\times$ 10^6 m^3/h, only a third of the estimate for the Northern 1998 lava flow. This is consistent with Flow K having a higher proportion of "inflated pillow flow" morphology.

4.3. Relation Between Eruption Rate and Lava Morphology

[43] Previous work has proposed a link between lava effusion rate and submarine lava morphology (generally referring to the photo-scale). Laboratory analog experiments have suggested that effusion rate is the most important control on submarine lava morphology, with pillows produced by slow extrusion and sheets produced by rapid effusion [*Griffiths and Fink*, 1992; *Gregg and Fink*, 1995; *Gregg et al*., 1996; *Gregg and Fink*, 2000]. Real-world confirmation of these results has been mixed. For example, *Fundis et al*. [2010] interpreted that effusion rate was indeed the dominant control on the morphology of lavas produced by the 2005–2006 eruption on the East Pacific Rise at 9–10°N, whereas *Gregg and Smith* [2003] showed that slope had a stronger influence on lava morphology than predicted in the lab. Our mapping results show that the sequence of events during lava flow emplacement is equally as important for understanding the initial formation and final distribution of lava morphologies on submarine lava flows. For example, the full range of photo-scale lava morphologies is present in the 1998 lava flows, but their proportions vary spatially and with distance from the eruptive vents. This study shows that map-scale flow morphology is critically important for interpreting submarine lava flow emplacement processes and estimating eruption rate, because it provides a meaningful context for observations of photo-scale lava morphology.

4.4. Comparison With the East Pacific Rise at 9–10°N

[44] The East Pacific Rise (EPR) at 9–10°N is another mid-ocean ridge study site that has been the target of interdisciplinary research for more than a decade [*Fornari et al*., 2012], has experienced recent eruptions [*Haymon et al*., 1993; *Soule et al*., 2007], and has been mapped at high-resolution [*Fornari et al*., 2004; *Ferrini et al*., 2007]. The crest of the EPR has been surveyed with Imagenex scanning-sonar on *Alvin* and the *ABE* AUV, with the DSL-120 sidescan sonar, and by visual observations from submersible dives and camera tows [*Kurras et al*., 2000; *Fornari et al*., 2004; *Escartin et al*., 2007; *Fundis et al*., 2010]. Both the EPR 9–10°N and Axial Seamount are in a seafloor spreading environment, but the physiographic settings are different. The EPR ridge crest at 9–10°N has a relatively uniform depth along its length (2520–2580 m) with slopes of 1–3° on the ridge flanks, whereas the setting at Axial includes a relatively flat-floored caldera and a rift zone with a steeper depth gradient along its length (1520–2300 m), reflecting that magma is centrally stored beneath the caldera and intruded into the rift zone by lateral dike injections [*Dziak and Fox*, 1999;

West et al., 2001; *Chadwick et al*., 2012]. Most lava flows on the EPR at 9–10°N are erupted from the axial summit trough at the ridge crest [*Fornari et al*., 1998; *Soule et al*., 2007]. Smaller eruptions flood and overflow the axial trough with lobate flows that inflate and drain out [*Gregg et al*., 1996]. Larger eruptions distribute lava 1–2 km off-axis in well-developed channels [*Soule et al*., 2005; *Soule et al*., 2007]. The larger flows form broad lobes with lobate morphology in their interiors and scalloped flow fronts of pillow lava at their terminal ends that are distinctive in sidescan imagery [*Fornari et al*., 2004; *Soule et al*., 2007; *Fundis et al*., 2010].

[45] These downslope flow fronts at the EPR at 9–10°N appear to be the equivalent of the distal inflated pillow flows that we have described at Axial. They may be more recognizable as a distinctive map-scale flow morphology at Axial because we have before-and-after-eruption multibeam bathymetry (ship-based for the 1998 eruption and AUV-based for the 2011 eruption [*Caress et al*., 2012]). The high-resolution AUV bathymetry reveals the morphology and thickness of the inflated pillow flows and makes it clear that they have fluid cores that thicken with lava from upslope, and thus that they form in a different way than other parts of the flows. In addition, inflated pillow flows may be more prominent in the 1998 and 2011 eruptions at Axial because they are larger in volume ($>31 \times 10^6$ m^3), compared to the smaller historical eruptions at the EPR at 9–10°N ($4–22 \times 10^6$ m^3) [*Gregg et al*., 1996; *Soule et al*., 2007].

4.5. Comparison Between the 1998 and 2011 Eruptions at Axial

[46] The April 2011 eruption at Axial Seamount reoccupied most of the same eruptive fissures that were active in 1998 [*Caress et al*., 2012], as well as older fissures between the Northern and Southern 1998 lava flows (Figure 16), including the one that fed the "pre-1982" flow in the Bag City vent area [*Clague et al*., 2013]. The northern limit of the eruptive fissures was about the same in 1998 and 2011, but the 2011 fissures are slightly offset to the east at their northern end so they extend up onto the caldera rim whereas the 1998 fissures were confined to the caldera floor. Between 45 53.8′N and 54.8′N, the 2011 eruptive fissures bridge the gap between the Northern and Southern 1998 lava flows (Figures 16a and 16b). Because their eruptive fissures were so similar, the 2011 lavas now cover 58% of the 1998 lava flows, by area (Figure 16c). The 2011 lava flows erupted in and near the caldera are similar in morphology to the 1998 lavas, in that they are primarily inflated lobate flows, 3–5 m thick, near the eruptive vents and inflated pillow flows up to 15 m thick at their distal ends [*Caress et al*., 2012]. Where 2011 lava covers 1998 flows on a slope (for example at the north end of the Northern 1998 flow) the 2011 lava mimics the fine-scale bathymetry of the underlying 1998 flows to a remarkable degree [*Caress et al*., 2012], suggesting that the 2011 lavas flooded the entire area and drained out so rapidly that they did not significantly alter the terrain. The 2011 lava added an increment of lava thickness everywhere, regardless of whether on uncollapsed flow tops or in the floors of collapse areas and channels. In contrast, on flat terrain, the 2011 lava filled in pre-existing collapses with lobate lava, such as north of the constriction in the middle section of the 1998 flow, in the Marker 33 vent area.

[47] The volume of lava erupted in and near the caldera was similar in 1998 and 2011 (31×10^6 m^3 in 1998 versus 33×10^6 m^3 in 2011), but the 2011 eruption is interpreted to have also included an eruption site located ~30 km south of the caldera on the south rift zone where another 66×10^6 m^3 was erupted [*Caress et al*., 2012]. Depth changes there between ship-based multibeam surveys collected in May 1998 and August 2011 were up to 138 m (with an average depth change of 30 m), which we interpret to be a "pillow ridge" with a length of 5 km and a width of 500 m. This pillow ridge is interpreted to be a product of the 2011 eruption because continuous seismo-acoustic and deformation monitoring between January 1998 and April 2011 detected no other signals indicative of an eruption [*Dziak et al*., 2011; *Caress et al*., 2012; *Chadwick et al*., 2012; *Dziak et al*., 2012]. Again, we acknowledge there is some ambiguity about whether there could have been an undetected eruption far down the south rift in 1998. If we assume that there was not, then the volume of lava erupted in 1998 was only 31% of the total volume erupted in 2011, even though the volume of magma removed from the summit reservoir in 1998 was more, based on deformation measurements [*Chadwick et al*., 2012]. This discrepancy could be because the 1998 eruption had a significantly higher ratio of dike-volume to erupted-volume than was the case in 2011.

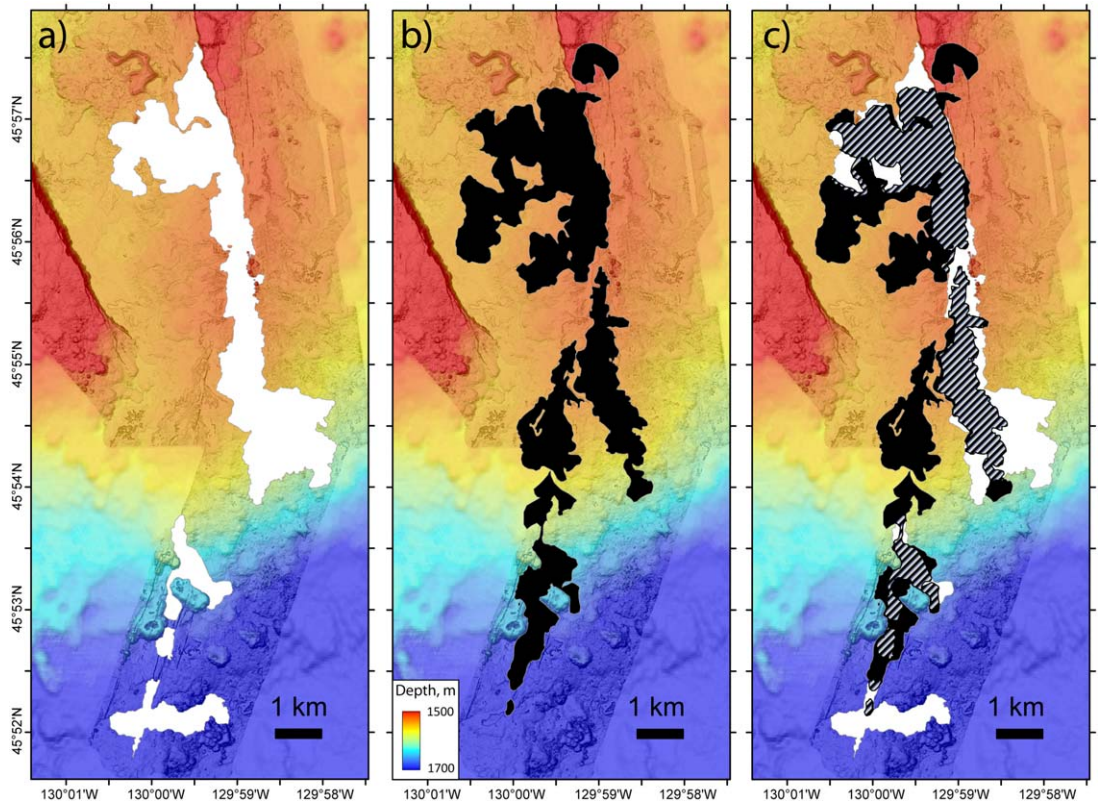

Figure 16. Comparison between 1998 and 2011 lava flow outlines along the upper south rift zone. (a) 1998 lava flows shown in white, (b) 2011 lava flows shown in black, (c) areas where 2011 lava buried 1998 lava shown with diagonal stripes. Note 2011 lava was also erupted ~30 km further south on the south rift [*Caress et al*., 2012].

[48] Another comparison that can be made between the 1998 and 2011 events is the timing of eruption related thermal and geophysical signals recorded by in situ and remote monitoring instruments (Table 2). Two bottom pressure recorders (BPRs) were in place in the caldera during both events [*Fox*, 1999; *Fox et al*., 2001; *Chadwick et al*., 2012]. Seismicity was monitored remotely by SOSUS hydrophone arrays in 1998 [*Dziak and Fox*, 1999] and by two in situ ocean-bottom hydrophones (OBHs) in 2011 [*Dziak et al*., 2012]. Additionally, miniature temperature recorders (MTRs) moored 15–115 m above the seafloor were in place near the eruption zone in 1998 [*Baker et al*., 1999]. The BPRs measured vertical movements of the seafloor related to magmatic inflation and deflation, and in both events we interpret that the eruption onset coincides with the start of deflation in the BPR records, based on abrupt temperature increases recorded by the BPRs and MTR arrays (Table 2), presumably due to molten lava on the seafloor nearby [*Baker et al*., 1999; *Fox et al*., 2001; *Chadwick et al*., 2012]. In both cases, an intense seismic swarm began 2–3 h before the eruption onset (3.3 h in 1998, and 2.6 h in 2011; Table 2), which *Dziak et al*. [2012] interpreted as caused by the vertical intrusion of a dike from the subcaldera magma reservoir to the surface. As the dike neared the seafloor, 7–34 cm of vertical uplift was recorded by the BPRs <1 h before the eruption onset (6–66 min in 1998, and 40 min in 2011; Table 2). The amount of dike-induced uplift was greatest and the duration of the uplift was shortest for BPRs closest to the eruptive fissures, consistent with models of surface deformation during dike intrusion [*Pollard et al*., 1983]. During both events, one BPR was located near the center of the caldera, 750–1750 m west of the northern-most eruptive fissures, and a second BPR was located in the SE caldera, 155–1100 m west of the eruptive fissures. In both eruptions, the onset of lava effusion (deflation) began 15–19 min earlier at the northern BPR than the southern BPR, consistent with the dike reaching the surface and opening first at the northern end of the eruptive fissures and then propagating southward. Thus, the eruption

Table 2. Comparison of the Timing of Instrumentally Recorded Events During the 1998 and 2011 Eruptions at Axial

Event	Year	Date/Time, GMT	Time Relative to Eruption Onset (hh:mm)[a]	Reference
Start of seismicity	1998	25 Jan, 11:33	−03:18	*Dziak and Fox* [1999]
	2011	6 Apr, 00:35	−02:35	*Dziak et al*. [2012]
Start of dike-induced uplift at caldera center[b]	1998	25 Jan, 13:45	−01:06	*Fox* [1999]; this study
	2011	6 Apr, 02:30	−00:40	*Chadwick et al*. [2012]
Start of dike-induced uplift in SE caldera[b]	1998	25 Jan, 14:45[c]	−00:06	*Fox et al*. [2001]; this study
	2011	6 Apr, 02:30	−00:40	*Chadwick et al*. [2012]
Start of deflation at caldera center[b]	1998	25 Jan, 14:51	00:00	*Fox* [1999]; this study
	2011	6 Apr, 03:10	00:00	*Chadwick et al*. [2012]
Start of deflation in SE caldera[b]	1998	25 Jan, 15:10[c]	+ 00:19	*Fox et al*. [2001]; this study
	2011	6 Apr, 03:25	+ 00:15	*Chadwick et al*. [2012]
Start of temperature increase on MTR mooring T41[d]	1998	25 Jan, 15:00–15:30[c]	+ 00:09–00:39	*Baker et al*. [1999]; this study

[a]Eruption onset is assumed to coincide with the start of deflation recorded at the center of the caldera.
[b]Start of dike-induced uplift and start of deflation are from bottom pressure recorder (BPR) data.
[c]Dike-induced deformation in the SE caldera in 1998 is interpreted to start with subsidence of 10 cm from 14:45–14:55, followed by uplift of 34 cm from 14:55–15:10, as measured by the VSM2 instrument. We assume that the end of dike-induced deformation at 15:10 marks the opening of the eruptive fissures. The VSM2 instrument then recorded rapid uplift at 15:16 and a temperature increase at 15:17 due to lava reaching the instrument.
[d]The first large and unmistakable temperature increase (1.1°C) on the T41 MTR mooring was at 15:30 (or between 15:00 and 15:30, since the sensors record every 30 min) and was measured on the lowest MTR (at 1505 m, only 15 m above the bottom). This timing is consistent with the VSM2 data showing an apparent eruption start at 15:10 and lava reaching the instrument at 15:16.

onsets were remarkably similar in 1998 and 2011. Also, the behavior of Axial Seamount appears to be analogous to other basaltic volcanoes with centralized magma reservoirs and radiating rift zones in that its eruptions are sourced beneath the summit caldera and are fed by blade-like dikes that propagate laterally down the rift zones [*Wright et al*., 2012]. The duration of the deflation recorded by the BPRs was 6 days in both 1998 and 2011 [*Fox*, 1999; *Chadwick et al*., 2012], placing an upper limit on the duration of any possible surface eruption, because it reflects the time during which magma was leaving the summit reservoir and entering the rift zone.

5. Conclusions

[49] 1. The 1998 eruption at Axial Seamount produced four lava flows that we mapped using ship-based multibeam sonar, 1 m resolution AUV bathymetry, sidescan imagery, and dive observations. We estimate the total erupted volume to be 31×10^6 m^3, and of that volume 70% was in the northern-most flow, 23% was in the southern-most flow, and 7% was in the two smaller flows in between.

[50] 2. The 1998 eruption was fed from 11 *en echelon* eruptive fissures, spanning a distance of 11 km in the SE caldera and the upper south rift zone. Snowblower vents were observed with ~50 m of the eruptive fissures on the Northern 1998 lava flow. Despite hydroacoustic evidence that a dike intruded 50 km down the south rift zone, there is no evidence that 1998 lava erupted south of the extent we have mapped.

[51] 3. Based on the nearly complete coverage of the 1998 flows with high-resolution bathymetry we distinguish two map-scale flow morphologies and propose a conceptual model for their formation. On the 1998 lavas, "inflated lobate flow" morphology with intricate drained channels generally formed near the eruptive vents. Where those flows subsequently drained more than 0.5–1 km downslope, the flow morphology transitioned to "inflated pillow flows." Inflated pillow flows locally display collapses in their cores from drain-out that reveal their internal lava distribution system, but at the downslope ends of flows they generally do not drain and so remain intact. "Pillow mounds or ridges" are a third distinct map-scale flow morphology that is characteristic of some other historical eruptions (including parts of the 2011 Axial flows), but did not form in the 1998 Axial flows. The main differences between these three morphologies are flow thickness, the relative size of molten lava cores during flow emplacement, the pattern and extent of collapse features, and distribution of photo-scale lava morphologies. We interpret that "pillow mounds" are produced by a low effusion rate, whereas "inflated lobate flows" and "inflated pillow flows" form during high effusion-rate eruptions.

[52] 4. The 1998 lava flows were probably emplaced rapidly (<12 h). The degree of drain-out and transformations in flow morphologies was a function of the underlying slope, the existence or absence of flow constrictions, and the distance

from the eruptive vents. On nearly flat seafloor, the amount of collapse was low (19%), whereas on slopes up to a few degrees the area of collapse increased to >50% as the flow transformed from inflated lobate flows to channelized sheet flows, and eventually to thick inflated pillow flows at the distal ends.

[53] 5. This eruption shows that the notion that photo-scale lava flow morphology is controlled primarily by eruption rate is oversimplified, because the 1998 lava flows contain the full range of photo-scale lava morphologies. In addition, the eruption rate at a vent almost certainly varies with time, and the local lava supply rate at an active flow front probably also varies with distance from the vent. Nevertheless, it is likely true that eruption rate controls at least the initial morphology of submarine lava flows as they first spread out from eruptive vents, such that slow extrusion forms pillows and rapid effusion forms lobate lava or sheets. However, the final morphology of a lava flow is also strongly influenced by local slope, eruption duration, and the sequence of events during emplacement, including inflation, drain-out, and collapse. The concept of map-scale morphology may be more meaningful for interpreting submarine lava flow emplacement and constraining eruption rate.

[54] 6. There are remarkable similarities between the 1998 and 2011 eruptions at Axial. These similarities include the timing of precursory geophysical signals during intrusion of magma to the surface, the location and extent of eruptive fissures in and near the caldera, the volume of lava erupted in the caldera and on the upper south rift, the inferred short duration of eruption, the map-scale morphology of the lava flows, the creation of snowblower vents within ~50 m of eruptive fissures, and the formation of a microbial-produced "eruption mat" on the surface of the new lava where it was thick (>2 m) and cooled slowly. Despite all these similarities, the 2011 eruption produced a pillow ridge ~30 km down the south rift with twice the volume erupted in and near the caldera that the 1998 eruption did not.

[55] 7. This study shows the value of archival seafloor mapping data sets for documenting subsequent changes due to historical eruptions; in our case, the mid-1980s sidescan imagery at Axial were critical to defining the full extent of the 1998 lava flows, even though the data's resolution and navigational accuracy are lower than modern systems. Finally, this study demonstrates that visual observations and high-resolution bathymetry are a powerful combination for geologic mapping on the seafloor and the interpretation of submarine eruptive processes during lava flow emplacement.

Acknowledgments

[56] Many colleagues provided assistance and insights during the numerous ROV expeditions to Axial Seamount between 1998 and 2011. Thanks also to Dan Scheirer for assistance with his Imagenex sonar processing software in the early stages of this work. Reviewers Dan Fornari and Tracy Gregg helped improve the manuscript. Support for this research was provided by the NOAA Vents Program, NOAA National Undersea Research Program, a grant from the David and Lucile Packard Foundation to the Monterey Bay Aquarium Research Institute, and National Science Foundation grant OCE-0725605. Peri Sasnett's contributions were performed under appointment to the NOAA Ernest F. Hollings Undergraduate Scholarship Program administered by Oak Ridge Associated Universities. PMEL contribution number 3964.

References

Appelgate, B. (1990), Volcanic and structural morphology of the southern flank of the Axial Volcano, Juan de Fuca Ridge: Results from a sea MARC I side scan sonar survey, *J. Geophys. Res.*, *95*(B8), 12,765–12,783.

Baker, E. T., C. G. Fox and J. P. Cowen (1999), In situ observations of the onset of hydrothermal discharge during the 1998 submarine eruption of Axial Volcano, Juan de Fuca Ridge, *Geophys. Res. Lett.*, *26*(23), 3445–3448.

Baker, E. T., R. P. Lowell, J. A. Resing, R. A. Feely, R. W. Embley, G. J. Massoth, and S. L. Walker (2004), Decay of hydrothermal output following the 1998 seafloor eruption at Axial Volcano: Observations and models, *J. Geophys. Res.*, *109*, B01205, doi:10.1029/2003JB002618.

Ballard, R. D., and T. H. van Andel (1977), Morphology and tectonics of the inner rift valley at 36°50'N on the Mid-Atlantic Ridge, *Geol. Soc. Am. Bull.*, *88*, 507–530.

Ballard, R. D., R. T. Holcomb, and T. H. van Andel (1979), The Galapagos Rift at 86°W: 3. Sheet flows, collapse pits, and lava lakes of the rift valley, *J. Geophys. Res.*, *84*, 5407–5422.

Ballard, R. D., R. Hekinian, and J. Francheteau (1984), Geological setting of hydrothermal activity at 12°50'N on the East Pacific Rise: A submersible study, *Earth Planet. Sci. Lett.*, *69*, 176–186.

Bruce, P. M., and H. E. Huppert (1989), Thermal control of basaltic fissure eruptions, *Nature*, *342*, 665–667.

Butterfield, D. A., G. J. Massoth, R. E. McDuff, J. E. Lupton, and M. D. Lilley (1990), Geochemistry of hydrothermal fluids from Axial Seamount hydrothermal emissions study vent field, Juan de Fuca Ridge: Subfloor boiling and subsequent fluid-rock interaction, *J. Geophys. Res.*, *95*(B8), 12,895–12,922.

Butterfield, D. A., K. K. Roe, M. D. Lilley, J. Huber, J. A. Baross, R. W. Embley, and G. J. Massoth (2004), Mixing, reaction and microbial activity in sub-seafloor revealed by temporal and spatial variation in diffuse flow vents at Axial Volcano, in *The Subseafloor Biosphere at Mid-Ocean*

Ridges, edited by W. S. D. Wilcock et al, pp. 269–289, AGU, Washington, D. C.

Caress, D. W., D. A. Clague, J. B. Paduan, W. W. Chadwick Jr., D. A. Butterfield, H. Thomas, D. Conlin, and D. Thompson (2007), AUV mapping of Axial Seamount, Juan de Fuca Ridge: The Northern Caldera Floor and Northeast Rim, *Eos Trans. AGU*, *88*(52), Fall Meet. Suppl., Abstract T33B-1355.

Caress, D. W., H. Thomas, W. J. Kirkwood, R. McEwen, R. Henthorn, E. A. Clague, C. K. Paull, J. Paduan, and K. L. Maier (2008), High-resolution multibeam, sidescan, and subbottom surveys using the MBARI AUV D. Allan B., in *Marine Habitat Mapping Technology for Alaska*, edited by J. R. Reynolds and H. G. Greene, Alaska Sea Grant Coll. Program, Univ. of Alaska, Fairbanks, Alaska.

Caress, D. W., D. A. Clague, J. B. Paduan, J. Martin, B. Dreyer, W. W. Chadwick Jr., A. Denny, and D. S. Kelley (2012), Repeat bathymetric surveys at 1-metre resolution of lava flows erupted at Axial Seamount in April 2011, *Nature Geosci.*, *5*(7), 483–488, doi:10.1038/NGEO1496.

Chadwick, J., M. Perfit, I. Ridley, I. Jonasson, G. Kamenov, W. W. Chadwick Jr., R. Embley, P. Le Roux, and M. Smith (2005), Magmatic effects of the Cobb Hotspot on the Juan de Fuca Ridge, *J. Geophys. Res.*, *110*, B03101, doi:10.1029/2003JB002767.

Chadwick, W. W. Jr. (2003), Quantitative constraints on the growth of submarine lava pillars from a monitoring instrument that was caught in a lava flow, *J. Geophys. Res.*, *108*(B11), 2534, doi:10.1029/2003JB002422.

Chadwick, W. W. Jr., and R. W. Embley (1994), Lava flows from a mid-1980s submarine eruption on the Cleft Segment, Juan de Fuca Ridge, *J. Geophys. Res.*, *99*(B3), 4761–4776.

Chadwick, W. W. Jr., R. W. Embley, and C. G. Fox (1995), SeaBeam depth changes associated with recent lava flows, CoAxial segment, Juan de Fuca Ridge: Evidence for multiple eruptions between 1981–1993, *Geophys. Res. Lett.*, *22*(2), 167–170.

Chadwick, W. W. Jr., R. W. Embley, and T. M. Shank (1998), The 1996 Gorda Ridge eruption: Geologic mapping, sidescan sonar, and SeaBeam comparison results, *Deep Sea Res., Part II*, *45*(12), 2547–2570.

Chadwick, W. W. Jr., T. K. P. Gregg, and R. W. Embley (1999a), Submarine lineated sheet flows: A unique lava morphology formed on subsiding lava ponds, *Bull. Volcanol.*, *61*, 194–206.

Chadwick, W. W. Jr., R. W. Embley, H. B. Milburn, C. Meinig, and M. Stapp (1999b), Evidence for deformation associated with the 1998 eruption of Axial Volcano, Juan de Fuca Ridge, from acoustic extensometer measurements, *Geophys. Res. Lett.*, *26*(23), 3441–3444.

Chadwick, W. W. Jr., D. S. Scheirer, R. W. Embley, and H. P. Johnson (2001), High-resolution bathymetric surveys using scanning sonars: Lava flow morphology, hydrothermal vents and geologic structure at recent eruption sites on the Juan de Fuca Ridge, *J. Geophys. Res.*, *106*(B8), 16,075–16,100.

Chadwick, W. W. Jr., R. W. Embley, and S. Merle (2002), Emplacement processes of two 1998 lava flows with contrasting morphology, inferred from high-resolution bathymetry and bottom observations at Axial Seamount, Juan de Fuca Ridge, *Eos Trans. AGU*, *83*(4), Ocean Sci. Meet. Suppl., Abstract OS41L-02.

Chadwick, W. W. Jr., S. Nooner, M. Zumberge, R. W. Embley, and C. G. Fox (2006), Vertical deformation monitoring at Axial Seamount since its 1998 eruption using deep-sea pressure sensors, *J. Volcanol. Geotherm. Res.*, *150*, 313–327.

Chadwick, W. W., Jr., S. L. Nooner, D. A. Butterfield, and M. D. Lilley (2012), Seafloor deformation and forecasts of the April 2011 eruption at Axial Seamount, *Nature Geosci.*, *5*(7), 474–477, doi:10.1038/NGEO1464.

Clague, D. A., D. W. Caress, J. B. Paduan, W. W. Chadwick Jr., D. A. Butterfield, H. Thomas, D. Conlin, and D. Thompson (2007), AUV mapping of Axial Seamount, Juan de Fuca Ridge: The Southern Caldera Floor and Upper South Rift, *Eos Trans. AGU*, *88*(52), Fall Meet. Suppl., Abstract T33B-1354.

Clague, D. A., et al. (2013), Geologic history of the summit of Axial Seamount, Juan de Fuca Ridge, *Geochem. Geophys. Geosyst.*, doi:10.1002/ggge.20240, in press.

Cormier, M.-H., W. B. F. Ryan, A. K. Shah, W. Jin, A. M. Bradley, and D. R. Yoerger (2003), Waxing and waning volcanism along the East Pacific Rise on a millennium time scale, *Geology*, *31*(7), 633–636.

Crane, K., and R. D. Ballard (1981), Volcanics and structure of the Famous Narrowgate Rift: Evidence for cyclic evolution: AMAR 1, *J. Geophys. Res.*, *86*(B6), 5112–5124.

Crowell, B. W., R. P. Lowell, and K. L. Von Damm (2008), A model for the production of sulfur floc and ''snowblower'' events at mid-ocean ridges, *Geochem. Geophys. Geosyst.*, *9*, Q10T02, doi:10.1029/2008GC002103.

Delaney, J. R., D. S. Kelley, M. D. Lilley, D. A. Butterfield, J. A. Baross, W. S. D. Wilcock, R. W. Embley, and M. Summit (1998), The quantum event of oceanic crustal accretion: Impacts of diking at mid-ocean ridges, *Science*, *281*, 222–230.

Desonie, D. L., and R. A. Duncan (1990), The Cobb-Eickelberg seamount chain: Hotspot volcanism with mid-ocean ridge basalt affinity, *J. Geophys. Res.*, *95*, 12,697–12,712.

Dziak, R. P., and C. G. Fox (1999), The January 1998 earthquake swarm at Axial Volcano, Juan de Fuca Ridge: Hydroacoustic evidence of seafloor volcanic activity, *Geophys. Res. Lett.*, *26*(23), 3429–3432.

Dziak, R. P., S. R. Hammond, and C. G. Fox (2011), A 20-year hydroacoustic time series of seismic and volcanic events in the Northeast Pacific Ocean, *Oceanography*, *24*(3), 280–293, doi:10.5670/oceanog.2011.79.

Dziak, R. P., J. H. Haxel, D. R. Bohnenstiehl, W. W. Chadwick Jr., S. L. Nooner, M. J. Fowler, H. Matsumoto, and D. A. Butterfield (2012), Seismic precursors and magma ascent before the April 2011 eruption at Axial Seamount, *Nature Geosci.*, *5*(7), 478–482, doi:10.1038/NGEO1490.

Embley, R. W., and W. W. Chadwick Jr. (1994), Volcanic and hydrothermal processes associated with a recent phase of seafloor spreading at the northern Cleft segment: Juan de Fuca Ridge, *J. Geophys. Res.*, *99*(B3), 4741–4760.

Embley, R. W., and E. T. Baker (1999), Interdisciplinary group explores seafloor eruption with remotely operated vehicle, *Eos Trans. AGU*, *80*(19), 213, 219, 222.

Embley, R. W., and J. E. Lupton (2004), Diking, event plumes and the subsurface biosphere at mid-ocean ridges, in *The Subseafloor Biosphere at Mid-Ocean Ridges*, edited by W. S. D. Wilcock et al., pp. 75–97, AGU, Washington, D. C.

Embley, R. W., K. M. Murphy, and C. G. Fox (1990), High resolution studies of the summit of Axial Volcano, *J. Geophys. Res.*, *95*, 12,785–12,812.

Embley, R. W., W. W. Chadwick Jr., D. Clague, and D. Stakes (1999), The 1998 eruption of Axial Volcano: Multibeam anomalies and seafloor observations, *Geophys. Res. Lett.*, *26*(23), 3425–2428.

Embley, R. W., W. W. Chadwick Jr., M. R. Perfit, M. C. Smith, and J. R. Delaney (2000), Recent eruptions on the

coaxial segment of the Juan de Fuca Ridge: Implications for mid-ocean ridge accretion processes, *J. Geophys. Res.*, *105*(B7), 16,501–16,525.

Emerson, D., and C. L. Moyer (2010), Microbiology of seamounts: Common patterns observed in community structure, *Oceanography*, *23*(1), 148–163.

Engels, J. L., M. H. Edwards, D. J. Fornari, M. R. Perfit, and J. R. Cann (2003), A new model for submarine volcanic collapse formation, *Geochem. Geophys. Geosyst.*, *4*(9), 1077, doi:10.1029/2002GC000483.

Escartin, J., S. A. Soule, D. J. Fornari, M. A. Tivey, H. Schouten, and M. R. Perfit (2007), Interplay between faults and lava flows in construction of the upper oceanic crust: The East Pacific Rise crest 9, *Geochem. Geophys. Geosyst.*, *8*, Q06005, doi:10.1029/2006GC001399.

Ferrini, V. L., D. J. Fornari, T. M. Shank, J. C. Kinsey, M. A. Tivey, S. A. Soule, S. M. Carbotte, L. L. Whitcomb, D. Yoerger, and J. Howland (2007), Submeter bathymetric mapping of volcanic and hydrothermal features on the East Pacific Rise crest at 9°50'N, *Geochem. Geophys. Geosyst.*, *8*, Q01006, doi:10.1029/2006GC001333.

Fornari, D. J. (1986), Submarine lava tubes and channels, *Bull. Volcanol.*, *48*, 291–298.

Fornari, D. J., R. M. Haymon, M. R. Perfit, T. K. P. Gregg, and M. H. Edwards (1998), Axial summit trough of the East Pacific Rise 9°N to 10°N: Geological characteristics and evolution of the axial zone on fast-spreading mid-ocean ridges, *J. Geophys. Res.*, *103*(B5), 9827–9855.

Fornari, D. J., et al. (2004), Submarine lava flow emplacement at the East Pacific Rise 9°50′N: Implications for uppermost ocean crust stratigraphy and hydrothermal fluid circulation, in *Mid-Ocean Ridges: Hydrothermal Interactions Between the Lithosphere and Oceans*, edited by C. R. German, J. Lin, and L. M. Parson, pp. 187–217, AGU, Washington, D. C.

Fornari, D. J., et al. (2012), The East Pacific Rise between 9°N and 10°N: Twenty-five years of integrated, multidisciplinary oceanic spreading center studies, *Oceanography*, *25*(1), 18–43.

Fox, C. G. (1999), In situ ground deformation measurements from the summit of Axial Volcano during the 1998 volcanic episode, *Geophys. Res. Lett.*, *26*(23), 3437–3440.

Fox, C. G., K. M. Murphy, and R. W. Embley (1988), Automated display and statistical analysis of interpreted deep-sea bottom photographs, *Mar. Geol.*, *78*, 199–216.

Fox, C. G., W. W. Chadwick Jr., and R. W. Embley (2001), Direct observation of a submarine volcanic eruption from a sea-floor instrument caught in a lava flow, *Nature*, *412*, 727–729.

Francheteau, J., T. Juteau, and C. Rangan (1979), Basaltic pillars in collapsed lava-pools on the deep ocean-floor, *Nature*, *281*, 209–211.

Fundis, A. T., S. A. Soule, D. J. Fornari, and M. R. Perfit (2010), Paving the seafloor: Volcanic emplacement processes during the 2005–2006 eruptions at the fast spreading East Pacific Rise, 9°50'N, *Geochem. Geophys. Geosyst.*, *11*, Q08024, doi:10.1029/2010GC003058.

Gilbert, L. A., R. E. McDuff, and H. P. Johnson (2007), Porosity of the upper edifice of Axial Seamount, *Geology*, *35*(1), 49–52.

Gregg, T. K. P., and W. W. Chadwick Jr. (1996), Submarine lava-flow inflation: A model for the formation of lava pillars, *Geology*, *24*(11), 981–984.

Gregg, T. K. P., and J. H. Fink (1995), Quantification of submarine lava-flow morphology through analog experiments, *Geology*, *23*(1), 73–76.

Gregg, T. K. P., and J. H. Fink (2000), A laboratory investigation into the effects of slope on lava flow morphology, *J. Volcanol. Geotherm. Res.*, *96*(3–4), 145–159.

Gregg, T. K. P., and D. K. Smith (2003), Volcanic investigations of the Puna Ridge, Hawaii: Relations of lava flow morphologies and underlying slopes, *J. Volcanol. Geotherm. Res.*, *126*, 63–77.

Gregg, T. K. P., D. J. Fornari, M. R. Perfit, R. M. Haymon, and J. H. Fink (1996), Rapid emplacement of a mid-ocean ridge lava flow on the East Pacific Rise at 9° 46'-51'N, *Earth Planet. Sci. Lett.*, *144*, E1–E7.

Griffiths, R. W., and J. H. Fink (1992), Solidification and morphology of submarine lavas: A dependence on extrusion rate, *J. Geophys. Res.*, *97*, 19,729–19,737.

Haymon, R. M. et al. (1993), Volcanic eruption of the mid-ocean ridge along the East Pacific Rise crest at 9° 45–52'N: Direct submersible observations of seafloor phenomena associated with an eruption event in April 1991, *Earth Planet. Sci. Lett.*, *119*, 85–101.

Heliker, C. C., and T. N. Mattox (2003), The first two decades of the Puu Oo-Kupaianaha eruption: Chronology and selected bibliography, in *The Puu Oo-Kupaianaha Eruption of Kilauea Volcano, Hawaii: The First 20 Years*, U. S. Geol. Surv. Prof. Pap. 1676, edited by C. C. Heliker, D. A. Swanson, and T. J. Takahashi, pp. 1–28, U.S. Geological Survey, Reston, VA.

Hon, K., J. Kauahikaua, R. Denlinger, and K. Mackay (1994), Emplacement and inflation of pahoehoe sheet flows: Observations and measurements of active lava flows on Kilauea volcano, Hawaii, *Geol. Soc. Am. Bull.*, *106*, 351–370.

Huber, J. A., D. A. Butterfield, and J. A. Baross (2003), Bacterial diversity in a subseafloor habitat following a deep-sea volcanic eruption, *FEMS Microb. Ecol.*, *43*(3), 393–409.

Huber, J. A., D. A. Butterfield, and J. A. Baross (2006), Diversity and distribution of subseafloor Thermococcales populations at an active deep-sea volcano in the Northeast Pacific Ocean, *J. Geophys. Res.*, *111*, G04016, doi:10.1029/2005JG000097.

Johnson, H. P., and R. W. Embley (1990), Axial Seamount: An active ridge axis volcano on the central Juan de Fuca Ridge, *J. Geophys. Res.*, *95*(B8), 12,689–12,696.

Juniper, S. K., P. Martineu, J. Sarrazin, and Y. Gélinas (1995), Microbial-mineral floc associated with nascent hydrothermal activity on CoAxial segment, Juan de Fuca Ridge, *Geophys. Res. Lett.*, *22*(2), 179–182.

Kent, G., A. Harding, J. Babcock, J. A. Orcutt, R. S. Detrick, J. P. Canales, E. M. Van Ark, S. M. Carbotte, J. Diebold, and M. Nedimovic (2003), A new view of 3-D magma chamber structure beneath axial seamount and coaxial segment: Preliminary results from the 2002 multichannel seismic survey of the Juan de Fuca Ridge, *Eos Trans. AGU*, *84*(46), Fall Meet. Suppl., Abstract B12A-0755.

Kouris, A., S. K. Juniper, G. Frébourg, and F. Gaill (2007), Protozoan-bacterial symbiosis in a deep-sea hydrothermal vent folliculinid ciliate (Folliculinopsis sp.) from the Juan de Fuca Ridge, *Mar. Ecol.*, *28*, 63–71.

Kouris, A., H. Limén, C. J. Stevens, and S. K. Juniper (2010), Faunal composition and food web structure in colonial ciliate (Folliculinopsis sp.) mats at northeast Pacific hydrothermal vents, *Mar. Ecol. Prog. Ser.*, *412*, 93–101.

Kurras, G. J., D. J. Fornari, M. H. Edwards, M. R. Perfit, and M. C. Smith (2000), Volcanic morphology of the East Pacific Rise crest 9°49'-52': Implications for volcanic emplacement processes at fast-spreading mid-ocean ridges, *Mar. Geophys. Res.*, *21*, 23–41.

Lockwood, J. P., J. J. Dvorak, T. T. English, R. Y. Koyanagi, A. T. Okamura, M. L. Summers, and W. R. Tanigawa (1987), Manua Loa 1974–1984: A decade of intrusive and extrusive activity, in *Volcanism in Hawaii*, U. S. Geol. Surv. Prof. Pap., 1350, edited by R. W. Decker, T. L. Wright, and P. H. Stauffer, pp. 537–570, U.S. Geological Survey, Reston, VA.

Lupton, J. E., E. T. Baker, R. W. Embley, R. Greene, and L. Evans (1999), Anomalous helium and heat signatures associated with the 1998 Axial Volcano event, Juan de Fuca Ridge, *Geophys. Res. Lett.*, *26*(23), 3449–3452.

Marcus, J., and S. Hourdez (2002), A new species of scaleworm (Polychaeta: Polynoidae) from Axial Volcano, Juan de Fuca Ridge, northeast Pacific, *Proc. Biol. Soc. Washington*, *115*(2), 341–349.

Marcus, J., V. Tunnicliffe, and D. A. Butterfield (2009), Post-eruption succession of macrofaunal communities at diffuse flow hydrothermal vents on Axial Volcano, Juan de Fuca Ridge, Northeast Pacific, *Deep Sea Res., Part II*, *56*, 1586–1598.

Meyer, J. L., N. H. Akerman, G. Proskurowski, and J. A. Huber (2013), Microbiological characterization of a post-eruption ''snowblower'' vents at Axial Seamount, Juan de Fuca Ridge, *Front. Microbiol.*, *4*, 153, doi:10.3389/fmicb.2013.00153.

Monterey Bay Aquarium Research Institute (2001), West coast seamounts and ridges multibeam survey, MBARI Digital Data Series, No. 7, Moss Landing, CA.

Moore, J. G. (1975), Mechanism of formation of pillow lava, *Am. Sci.*, *63*, 269–277.

Moyer, C. L., and J. J. Engebretson (2002), Colonization by pioneer populations of epsilon-Proteobacteria and community succession at mid-ocean ridge hydrothermal vents as determined by T-RFLP analysis, *Eos Trans. AGU*, *83*(47), Fall Meet. Suppl., Abstract V11C-12.

Nooner, S. L., and W. W. Chadwick Jr. (2009), Volcanic inflation measured in the caldera of Axial Seamount: Implications for magma supply and future eruptions, *Geochem. Geophys. Geosyst.*, *10*, Q02002, doi:10.1029/2008GC002315.

Opatkiewicz, A. D., D. A. Butterfield, and J. A. Baross (2009), Individual hydrothermal vents at Axial Seamount harbor distinct subseafloor microbial communities, *FEMS Microb. Ecol.*, *70*, 413–424.

Perfit, M. R., and W. W. Chadwick Jr. (1998), Magmatism at mid-ocean ridges: Constraints from volcanological and geochemical investigations, in *Faulting and Magmatism at Mid-Ocean Ridges*, edited by W. R. Buck et al., pp. 59–116, AGU, Washington, D. C.

Perfit, M. R., D. J. Fornari, M. C. Smith, J. F. Bender, C. H. Langmuir, and R. M. Haymon (1994), Small-scale spatial and temporal variations in mid-ocean ridge crest magmatic processes, *Geology*, *22*, 375–379.

Peterson, D. W., R. T. Holcomb, R. I. Tilling, and R. L. Christiansen (1994), Development of lava tubes in the light of observations at Mauna Ulu, Kilauea Volcano, *Hawaii, Bull. Volcanol.*, *56*, 343–360.

Pollard, D. D., P. T. Delaney, P. T. Duffield, E. T. Endo, and A. T. Okamura (1983), Surface deformation in volcanic rift zones, *Tectonophysics*, *94*(1–4), 541–584.

Resing, J. A., R. Feely, G. Massoth, and E. T. Baker (1999), The water-column chemical signature after the 1998 eruption of Axial Volcano, *Geophys. Res. Lett.*, *26*(24), 3645–3648.

Rhodes, J. M., C. Morgan, and R. A. Liias (1990), Geochemistry of Axial Seamount lavas: Magmatic relationship between the Cobb Hotspot and the Juan de Fuca Ridge, *J. Geophys. Res.*, *95*(B8), 12,713–12,734.

Rubin, K. H., J. D. Macdougall, and M. R. Perfit (1994), ^{210}Po-^{210}Pb dating of recent volcanic eruptions on the seafloor, *Nature*, *368*, 841–844.

Sinton, J. M., E. Bergmanis, K. Rubin, R. Batiza, T. K. P. Gregg, K. Gronvold, K. C. Macdonald, and S. M. White (2002), Volcanic eruptions on mid-ocean ridges: New evidence from the superfast spreading East Pacific Rise, 17°-19°S, *J. Geophys. Res.*, *107*(B6), 2115, doi:10.1029/2000JB000090.

Smith, D. K., and J. R. Cann (1992), The role of seamount volcanism in crustal construction at the Mid-Atlantic Ridge (24°-30°N), *J. Geophys. Res.*, *97*(B2), 1645–1658.

Sohn, R. A., A. H. Barclay, and S. C. Webb (2004), Microearthquake patterns following the 1998 eruption of Axial Volcano, Juan de Fuca Ridge: Mechanical relaxation and thermal strain, *J. Geophys. Res.*, *109*, B01101, doi:10.1029/2003JB002499.

Soule, S. A., D. J. Fornari, M. R. Perfit, M. A. Tivey, W. I. Ridley, and H. Schouten (2005), Channelized lava flows at the East Pacific Rise crest 9°–10°N: The importance of off-axis lava transport in developing the architecture of young oceanic crust, *Geochem. Geophys. Geosyst.*, *6*, Q08005, doi:10.1029/2005GC000912.

Soule, S. A., D. J. Fornari, M. R. Perfit, and K. H. Rubin (2007), New insights into mid-ocean ridge volcanic processes from the 2005–2006 eruption of the East Pacifi c Rise, 9°46′N–9°56′N, *Geology*, *35*(12), 1079–1082.

Soule, S. A., J. Escartin, and D. J. Fornari (2009), A record of eruption and intrusion at a fast spreading ridge axis: Axial summit trough of the East Pacific Rise at 9–10°, *Geochem. Geophys. Geosyst.*, *10*, Q10T07, doi:10.1029/2008GC002354.

Tolstoy, M., F. L. Vernon, J. A. Orcutt, and F. K. Wyatt (2002), Breathing of the seafloor: Tidal correlations of seismicity at Axial volcano, *Geology*, *30*(6), 503–506.

Wadge, G. (1981), The variation of magma discharge during basaltic eruptions, *J. Volcanol. Geotherm. Res.*, *11*, 139–168.

West, M. E., W. Menke, M. Tolstoy, S. Webb, and R. Sohn (2001), Magma storage beneath Axial Volcano on the Juan de Fuca mid-ocean ridge, *Nature*, *413*, 833–836.

White, S. M., K. C. Macdonald, and R. M. Haymon (2000), Basaltic lava domes, lava lakes, and volcanic segmentation on the southern East Pacific Rise, *J. Geophys. Res.*, *103*(B10), 25,519–25,536.

White, S. M., K. C. Macdonald, and J. M. Sinton (2002), Volcanic mound fields on the East Pacific Rise, 16°-19°S: Low effusion rate eruptions at overlapping spreading centers for the past 1 Myr, *J. Geophys. Res.*, *107*(B10), 2240, doi:10.1029/2001JB000483.

White, S. M., J. D. Meyer, R. M. Haymon, K. C. Macdonald, E. T. Baker, and J. A. Resing (2008), High-resolution surveys along the hot spot—affected Galapagos Spreading Center: 2. Influence of magma supply on volcanic morphology, *Geochem. Geophys. Geosyst.*, *9*, Q09004, doi:10.1029/2008GC002036.

White, S. M., J. L. Mason, K. C. Macdonald, M. R. Perfit, V. D. Wanless, and E. M. Klein (2009), Significance of widespread low effusion rate eruptions over the past 2 million years for delivery of magma to the overlapping spreading

centers at 9°N East Pacific Rise, *Earth Planet. Sci. Lett.*, *280*, 175–184.

Wright, T. J. et al. (2012), Geophysical constraints on the dynamics of spreading centres from rifting episodes on land, *Nature Geosci.*, *5*, 242–250.

Wylie, J. J., K. R. Helfrich, B. Dade, J. R. Lister, and J. F. Salzig (1999), Flow localization in fissure eruptions, *Bull. Volcanol.*, *60*(6), 432–440.

Yeo, I., R. C. Searle, K. L. Achenbach, T. P. Le Bas, and B. J. Murton (2012), Eruptive hummocks: Building blocks of the upper ocean crust, *Geology*, *40*(1), 91–94.

Yeo, I. A., D. A. Clague, J. F. Martin, J. B. Paduan, and D. W. Caress (2013), Pre-eruptive flow focussing in dikes feeding historic pillow ridges on the Juan de Fuca and Gorda Ridges, *Geochem. Geophys. Geosyst.*, doi:10.1002/ggge.20210, in press.